International Journal of Multiphase Flow 36 (2010) 25–39

Contents lists available at ScienceDirect

International Journal of Multiphase Flow

journal homepage: www.elsevier.com/locate/ijmulflow

Comparison of several models for multi-size bubbly flows on an adiabatic experiment

Christophe Morel [a,*], Pierre Ruyer [b,1], Nathalie Seiler [c,2], Jérôme M. Laviéville [d,3]

[a] CEA, DEN, DER/SSTH/LMDL, 17 rue des Martyrs, F-38054 Grenoble, France
[b] IRSN, DPAM/SEMCA/LEMAR, Cadarache, Bât 700, BP 3 – 13 115 Saint Paul lez Durance Cedex, France
[c] IRSN DPAM/SEMCA/LEMAR, CEN Cadarache, Bât 700, 13 115 Saint Paul lez Durance Cedex, France
[d] Electricité de France R&D Division, 6 Quai Watier, F-78400 Chatou, France

ARTICLE INFO

Article history:
Received 16 December 2008
Received in revised form 19 June 2009
Accepted 1 September 2009
Available online 12 September 2009

Keywords:
Bubbly flow
Multiple size
Polydisperse
MTLOOP
NEPTUNE

ABSTRACT

This paper deals with the modelling and numerical simulation of *isothermal bubbly flows with multi-size bubbles*. The study of isothermal bubbly flows without phase change is a first step towards the more general study of boiling bubbly flows. Here, we are interested in taking into account the features of such isothermal flow associated to the multiple sizes of the different bubbles simultaneously present inside the flow. With this aim, several approaches have been developed. In this paper, two of these approaches are described and their results are compared to experimental data, as well as to those of an older approach assuming a single average size of bubbles. These two approaches are (i) the moment density approach for which two different expressions for the bubble diameter distribution function are proposed and (ii) the multi-field approach. All the models are implemented into the NEPTUNE_CFD code and are compared to a test performed on the MTLOOP facility. These comparisons show their respective merits and shortcomings in their available state of development.

1. Introduction

This paper deals with the modelling and the numerical simulation of *isothermal multi-size bubbly flows*. Several physical phenomena determine the bubble size and shape, which in turn determines the evolution of the flow structure (void fraction distribution, mean liquid and gas velocity profiles, turbulence intensity in the liquid phase...). The phenomena responsible for the changes in the bubble size distribution are the bubbles coalescence and break-up, the gas compressibility, the phase change and the bubbles deformations. Here, we will assume that the bubbles remain *spherical*, for the sake of simplicity. However, when the bubbles distort (i.e. they do not retain their spherical shape), the interface becomes anisotropic and a full tensorial treatment should be adopted (Doi and Ohta, 1991; Wetzel and Tucker, 1999; Lhuillier, 2004a,b; Morel, 2007). This general approach is very complicated, and only few closures are available in the literature in very restricted cases. Therefore, for this first study, we assume that the bubbles remain spherical. In fact, in all the approaches that will be presented here, the bubbles are supposed to be multi-dispersed in size but not in shape. The general study of bubbly flows with bubbles multi-dispersed in size and in shape could be envisaged in a future work.

It is also assumed that there is no phase change, therefore only the first three types of physical phenomena (coalescence, break-up and gas compressibility) will influence the bubble diameter. Indeed, we consider isothermal flows without phase change as a first stage with the aim of evaluating the different approaches for the prediction of bubbly flows with multi-size bubbles, and that, although some of these methods have already been tested in boiling bubbly flow studies (Seiler and Ruyer, 2008; Morel and Laviéville, 2008).

The simultaneous existence of several bubble sizes in a bubbly flow has direct consequences on the velocities. In a quiescent liquid, it is observed that the bubble rising velocity generally depends on the bubble size: the larger the bubble, the greater the bubble rising velocity. If we consider a more complex flow, with a vertical liquid flow rate, and define the bubble relative velocity as the difference between the bubble velocity and the velocity of the surrounding liquid, this relative velocity depends on the bubble size in the same manner. This difference between the relative velocities of bubbles having different sizes is known as a possible source of bubble collisions and coalescences (Prince and Blanch, 1990). Another important aspect for upward bubbly

* Corresponding author. Tel.: +33 4 38 78 92 27; fax: +33 4 38 78 94 53.
E-mail addresses: christophe.morel@cea.fr (C. Morel), pierre.ruyer@irsn.fr (P. Ruyer), nathalie.seiler@irsn.fr (N. Seiler), jerome-marcel.lavieville@edf.fr (J.M. Laviéville).
[1] Tel.: +33 4 42 19 97 20.
[2] Tel.: +33 4 42 19 96 01.
[3] Tel.: +33 (0)1 30 87 84 49; fax: +33 (0)1 30 87 79 16.

0301-9322/$ - see front matter © 2009 Elsevier Ltd. All rights reserved.
doi:10.1016/j.ijmultiphaseflow.2009.09.003

flows in vertical pipes is that the small bubbles move laterally towards the pipe wall, and the large bubbles (above a critical size) move laterally in the opposite sense, i.e. towards the pipe axis. These various behaviours have been observed experimentally by many authors. Tomiyama (1998) relates this behaviour to the change of sign of the lift force, which is responsible for the lateral bubble migration, and proposes an empirical correlation to express the lift coefficient as a function of the bubble diameter (via the bubble Reynolds and Eotvos numbers). These two phenomena illustrate also the fact that a bubbly flow with multi-size bubbles is generally characterized also by bubble multiple velocities. In some approaches, like the multi-field approach presented in Section 6, this multi-velocity aspect can be taken into account in a very natural way but is tacked with more difficulties by other approaches, like with the moment density approaches described in Sections 4 and 5.

This paper is organized as follows. In Section 2, we briefly recall the two-fluid model in its simplified version for isothermal flows without phase change and the evolution equations for the different useful moment densities of the bubble diameter distribution function. All the presented approaches here can be derived from the equations established in Section 2, except for the multi-field approach, whose bases will be detailed in Section 6. Section 3 is devoted to the classical *single-size* approach, in which an *interfacial area concentration* (IAC) evolution equation is included. This IAC is combined with the bubble void fraction to determine the bubble *Sauter mean diameter* (SMD) which is the single diameter considered in this approach, called besides "single size". Two different approaches, namely the *moment's density approach* and the *multi-field one*, are frequently considered for the CFD simulations of bubbly flows with multiple bubble sizes. Two Sections 4 and 5 are devoted to various versions of the moment's density approach, and Section 6 is devoted to the multi-field approach. Simulations of a MTLOOP experiment have allowed comparing results of the various approaches and deducing their merits and shortcomings. This experiment will be described in Section 7. One experimental test is calculated with these four different approaches implemented into the NEPTUNE_CFD code. The results of the comparisons are presented in Section 8. In Section 9, some conclusions are drawn about the present status of the different methods and some perspectives are given for future work.

2. Two-fluid model and geometrical balance equations

In this paper, we deal with adiabatic and isothermal bubbly flows without phase change. In this situation, the mass and momentum balance equations of the two-fluid model read (Ishii and Hibiki, 2006):

$$\begin{aligned} &\frac{\partial \alpha_k \rho_k}{\partial t} + \nabla.(\alpha_k \rho_k \underline{V}_k) = 0 && k = L, G \\ &\frac{\partial \alpha_k \rho_k \underline{V}_k}{\partial t} + \nabla.(\alpha_k \rho_k \underline{V}_k \underline{V}_k) = -\alpha_k \underline{\nabla} p_k + \underline{M}_k + \alpha_k \rho_k \underline{g} && \\ &\qquad\qquad + \nabla.[\alpha_k (\underline{\underline{\tau}}_k + \underline{\underline{\tau}}_k^T)] && k = L, G \end{aligned} \tag{1}$$

where α_k is the local time-fraction of presence of phase k, ρ_k its averaged density, $\underline{V}_k$ its averaged velocity and p_k the bulk-averaged pressure for phase k. The vector $\underline{g}$ is the gravity acceleration, $\underline{\underline{\tau}}_k$ and $\underline{\underline{\tau}}_k^T$ are the averaged viscous stress tensor and the turbulent "Reynolds" stress tensor, respectively, and the vector $\underline{M}_k$ is the averaged interfacial transfer of momentum. The phase index k takes the values L for the liquid phase and G for the gas phase. Eqs. (1) have been obtained by Ishii and Hibiki (2006) by means of a time-averaging, but very similar equations can be obtained by means of ensemble averaging (e.g. Drew and Passman, 1999). The difference between the interfacial-averaged pressure for phase k p_{ki} and the bulk-averaged pressure p_k has been neglected. We will also neglect the difference between the two bulk-averaged pressures in the two phases, therefore making the approximation $p_L = p_G = p$.

Making this approximation of a common pressure for the two phases, the closure issue of the system of equations (1) lies in the averaged viscous stress tensors for the two phases, the Reynolds stress tensors for the two phases and the interfacial momentum transfers. Here we will describe only the closure of this last term (see also Section 8). If we neglect the averaged effects of the interfacial tension, the averaged interfacial momentum balance reduces to (Ishii and Hibiki, 2006):

$$\sum_{k=L,G} \underline{M}_k = 0 \tag{2}$$

Therefore it is sufficient to express the gas (or liquid) interfacial momentum transfer term, the liquid (or gas) interfacial momentum transfer being deduced from the action and reaction principle, in the context of the assumptions mentioned above. In bubbly flow studies, the interfacial momentum transfer term $\underline{M}_k$ is often decomposed into several averaged forces, namely a drag force, an added mass force, a lift force, a turbulent dispersion force and sometimes a wall force. The averaged expressions of these forces can be obtained approximately by averaging classical expressions for the forces exerted by the liquid on a single spherical bubble (e.g. Morel et al., 2004). These different forces involve the bubble diameter, therefore their averaged counterparts involve some geometrical moments of the bubble diameter distribution function, like the void fraction, the IAC and some averaged bubble diameters. It is therefore necessary to determine these geometrical moments in order to close the interfacial momentum transfer term. It is worthwhile to note that, in more general boiling bubbly flows involving phase change, the IAC or other geometrical variables also strongly influence the heat and mass interfacial transfers, hence the great importance given to their correct modelling.

As the bubbles remain spherical, the geometry of the bubbles population can be completely described by means of a distribution function $f(\xi;\underline{x},t)$ where ξ is a parameter characteristic of the bubble size, such as its diameter, its interfacial area or its volume. The bubble distribution function $f(\xi;\underline{x},t)$ is defined such that $f(\xi;\underline{x},t)\delta\xi\delta^3x$ is the probable number of bubbles having a size parameter between ξ and $\xi + \delta\xi$ into the volume element δ^3x around the point $\underline{x}$ at time t. Here we choose the bubble diameter d being the parameter ξ. The mean geometry of the bubble population can also be derived from the statistical moment densities of the distribution function. The pth-order moment density of the diameter distribution function is defined by:

$$S_p(\underline{x},t) \;\hat{=}\; \int d^p f(d;\underline{x},t)\delta d \tag{3}$$

We can construct an infinite number of mean diameters d_{pq} by using an infinite number of moment densities, through the definition relation:

$$d_{pq} \hat{=} \left(\frac{S_p}{S_q}\right)^{\frac{1}{p-q}} \tag{4}$$

The first four moment densities are related, under some assumptions regarding their spatial variation, to very useful quantities for the study of bubbly flows with spherical bubbles:

$$n \;\hat{=}\; S_0, \quad d_{10} \;\hat{=}\; S_1/n, \quad a_i \hat{=} \pi S_2, \quad \alpha \hat{=} \pi S_3/6 \tag{5}$$

where $n(\underline{x},t)$ is the bubble number density, $d_{10}(\underline{x},t)$ is the mean bubble diameter (mathematical expectation), $a_i(\underline{x},t)$ is the interfacial area concentration (IAC) and $\alpha(\underline{x},t)$ is the void fraction (averaged volumetric fraction of the gas phase). Three other important mean diameters are often used:

$$d_{20}=\left(\frac{S_2}{S_0}\right)^{\frac{1}{2}}=\sqrt{\frac{a_i}{\pi n}},\quad d_{30}=\left(\frac{S_3}{S_0}\right)^{\frac{1}{3}}=\left(\frac{6\alpha}{\pi n}\right)^{\frac{1}{3}},\quad d_{32}=\frac{S_3}{S_2}=\frac{6\alpha}{a_i} \tag{6}$$

The diameters d_{20} and d_{30} are called the mean surface diameter and the mean volume diameter, respectively (Oesterlé, 2006) and the last one, d_{32}, is the so-called Sauter mean diameter. In the "single-size" bubble approach, the Sauter mean bubble diameter is often used, because it depends directly on the void fraction, which is obtained as part of the solution of the system (1), and on the IAC which is obtained from an additional balance equation.

It can be shown, in a very general manner, that the bubble diameter distribution function $f(d;\underline{x},t)$ obeys to a Liouville–Boltzmann type equation (Hulburt and Katz, 1964; Achard, 1978):

$$\frac{\partial f}{\partial t}+\nabla.(f\,\underline{v}(d;\underline{x},t))+\frac{\partial fG(d;\underline{x},t)}{\partial d}=B^+(d;\underline{x},t)-B^-(d;\underline{x},t)+C^+(d;\underline{x},t)-C^-(d;\underline{x},t) \tag{7}$$

where $\underline{v}(d;\underline{x},t)$ is the velocity of a bubble having a diameter d, $G(d;\underline{x},t)$ is the bubble growth velocity of the same bubble measured along its trajectory, and B^+, B^-, C^+ and C^- are bubble source (+) and sink (−) terms due to bubble break-up (B) and coalescence (C), respectively. By introducing the velocity $\underline{v}(d;\underline{x},t)$, we implicitly assume no dispersion in bubble velocity for a given size but possible size related dispersion. These terms can be expressed by integral expressions (e.g. Kalkach-Navarro et al., 1994; Kocamustafaogullari and Ishii, 1995). At this time of our discussion, it is not useful to detail their expressions. In isothermal flows without phase change, the bubble growth rate G is only due to the gas compressibility. The p th-order moment density balance equation is obtained by making the product of Eq. (7) by d^p and integrating over all possible diameters. This gives:

$$\frac{\partial S_p}{\partial t}+\nabla.(S_p\underline{V}_p)-pG_{p-1}S_{p-1}=B_p^+-B_p^-+C_p^+-C_p^- \tag{8}$$

with the following definitions of the mean quantities appearing in Eq. (8):

$$\underline{V}_p\hat{=}\frac{\int\underline{v}(d;\underline{x},t)d^pf(d;\underline{x},t)\delta d}{\int d^pf(d;\underline{x},t)\delta d},\quad G_p\hat{=}\frac{\int G(d;\underline{x},t)d^pf(d;\underline{x},t)\delta d}{\int d^pf(d;\underline{x},t)\delta d},\quad B_p^+\hat{=}\int B^+(d;\underline{x},t)d^p\delta d \tag{9}$$

and similar definitions for the three last terms in Eq. (8). This equation has been derived by many authors (e.g. Kamp et al., 2001; Oesterlé, 2006) and is the basis for the derivation of different useful geometrical moment densities balance equations. Making successively $p=0,1,2,3$ in the general equation (8), and using the definitions (5), the four balance equations for the bubble number density n, the product of the bubble number density by the mean diameter nd_{10}, the interfacial area concentration a_i and the void fraction α are obtained:

$$\begin{aligned}&\tfrac{\partial n}{\partial t}+\nabla.(n\underline{V}_0)=B_0^+-B_0^-+C_0^+-C_0^-\\&\tfrac{\partial nd_{10}}{\partial t}+\nabla.(nd_{10}\underline{V}_1)-G_0S_0=B_1^+-B_1^-+C_1^+-C_1^-\\&\tfrac{\partial a_i}{\partial t}+\nabla.(a_i\underline{V}_2)-2\pi G_1nd_{10}=\pi(B_2^+-B_2^-+C_2^+-C_2^-)\\&\tfrac{\partial\alpha}{\partial t}+\nabla.(\alpha\underline{V}_3)-\tfrac{G_2}{2}a_i=0\end{aligned} \tag{10}$$

where the RHS (right-hand side) of the last equation (10) is zero because, when the whole bubble population is considered, the coalescence and break-up do not change the total amount of gas.

3. Single-size approach for bubbly flows

The single-size approach for bubbly flows has been used by many authors (Guido-Lavalle and Clausse, 1991; Kalkach-Navarro et al., 1994; Guido-Lavalle et al., 1994; Kocamustafaogullari and Ishii, 1995; Wu et al., 1998; Hibiki and Ishii, 2000; Lhuillier et al., 2000; Yao and Morel, 2004). This simplified approach consists in assuming that, locally, all the bubbles have the same diameter which can be given by the Sauter mean diameter. With this assumption, the bubble number density and the mean bubble diameter are given by the following relations:

$$n=\frac{\alpha}{\frac{\pi d^3}{6}}=\frac{1}{36\pi}\frac{a_i^3}{\alpha^2},\qquad d=d_{32}=\frac{6\alpha}{a_i} \tag{11}$$

Another assumption in this single-size approach is that the four mean velocities $\underline{V}_0$ to $\underline{V}_3$ appearing in Eqs. (10) are equal. Therefore, in this paragraph, we denote this common velocity by $\underline{V}_G$. The main assumptions being derived, we can give the closure for the bubble growth rate G due to the gas compressibility.

Let $D(\underline{x},t)$ be the bubble diameter in physical space (the notation d stands for the bubble diameter in phase space). In the absence of phase change, the bubble mass is conserved along its trajectory. As a consequence, the bubble diameter variation and the gas density variation measured along the bubble path are related through:

$$\frac{D(D)}{Dt}=-\frac{D}{3\rho}\frac{D\rho}{Dt} \tag{12}$$

where ρ denotes the gas density. The quantity G appearing in Eq. (7) is the conditional expectation of the Lagrangian derivative given by (12) conditioned by the equality $D(\underline{x},t)=d$:

$$G=\left\langle\frac{D(D)}{Dt}\middle|D=d\right\rangle=-\frac{d}{3}\left\langle\frac{1}{\rho}\frac{D\rho}{Dt}\middle|D=d\right\rangle\cong-\frac{d}{3}\frac{1}{\rho_G}\left(\frac{\partial\rho_G}{\partial t}+\underline{V}_G.\nabla\rho_G\right) \tag{13}$$

If we assume that the gas density ρ does not depend on the bubble diameter D, the conditional average appearing in the second expression of Eq. (13) can be replaced by the unconditional one. The last equality in Eq. (13) simply assumes that we neglect non-linear effect when we average the two terms under the brackets, therefore keeping only first order effects. Now, we can calculate the terms G_0 to G_2 appearing in Eqs. (10) from the definition $(9)_2$, we obtain:

$$\begin{aligned}G_0&=-\tfrac{1}{3\rho_G}\left(\tfrac{\partial\rho_G}{\partial t}+\underline{V}_G.\nabla\rho_G\right)\tfrac{S_1}{S_0}\\G_1&=-\tfrac{1}{3\rho_G}\left(\tfrac{\partial\rho_G}{\partial t}+\underline{V}_G.\nabla\rho_G\right)\tfrac{S_2}{S_1}\\G_2&=-\tfrac{1}{3\rho_G}\left(\tfrac{\partial\rho_G}{\partial t}+\underline{V}_G.\nabla\rho_G\right)\tfrac{S_3}{S_2}\end{aligned} \tag{14}$$

Substituting relations (14) into Eqs. (10) and using the definitions (5) gives:

$$\begin{aligned}&\tfrac{\partial n}{\partial t}+\nabla.(n\underline{V}_G)=B_0^+-B_0^-+C_0^+-C_0^-\\&\tfrac{\partial S_1}{\partial t}+\nabla.(S_1\underline{V}_G)=-\tfrac{1}{3\rho_G}\left(\tfrac{\partial\rho_G}{\partial t}+\underline{V}_G.\nabla\rho_G\right)S_1+B_1^+-B_1^-+C_1^+-C_1^-\\&\tfrac{\partial a_i}{\partial t}+\nabla.(a_i\underline{V}_G)=-\tfrac{2a_i}{3\rho_G}\left(\tfrac{\partial\rho_G}{\partial t}+\underline{V}_G.\nabla\rho_G\right)+\pi(B_2^+-B_2^-+C_2^+-C_2^-)\\&\tfrac{\partial\alpha}{\partial t}+\nabla.(\alpha\underline{V}_G)+\tfrac{\alpha}{\rho_G}\left(\tfrac{\partial\rho_G}{\partial t}+\underline{V}_G.\nabla\rho_G\right)=0\end{aligned} \tag{15}$$

It can be seen that the last equation (15) is the same as the first equation (1) where we put $k=G$, therefore the last equation (15) is redundant since we simply retrieve the mass balance equation for the gas phase. Using this equation into the preceding one $(15)_3$, the equation for the IAC can be rewritten into the following equivalent manner:

$$\frac{\partial a_i}{\partial t}+\nabla.(a_i\underline{V}_G)=\frac{2a_i}{3\alpha}\left(\frac{\partial\alpha}{\partial t}+\nabla.(\alpha\underline{V}_G)\right)+\pi(B_2^+-B_2^-+C_2^+-C_2^-) \tag{16}$$

It can also be seen, *under the assumptions retained here*, that the coalescence and break-up terms in Eqs. $(15)_1$ and (16) are not independent, since we can write for spherical bubbles (Lhuillier, 2004b):

$$\pi(B_2^+ - B_2^- + C_2^+ - C_2^-) = \frac{a_i}{3n}(B_0^+ - B_0^- + C_0^+ - C_0^-) = 12\pi\left(\frac{\alpha}{a_i}\right)^2 (B_0^+ - B_0^- + C_0^+ - C_0^-) \quad (17)$$

Substituting Eq. (17) into Eq. (16), we obtain the following final form:

$$\frac{\partial a_i}{\partial t} + \nabla.(a_i \underline{V}_G) = \frac{2a_i}{3\alpha}\left(\frac{\partial \alpha}{\partial t} + \nabla.(\alpha \underline{V}_G)\right) + 12\pi\left(\frac{\alpha}{a_i}\right)^2 (B_0^+ - B_0^- + C_0^+ - C_0^-) \quad (18)$$

which was derived independently by Hibiki and Ishii (2000).

Since the different geometrical quantities are related by Eqs. (11) in the single-size approach, it is completely equivalent to use Eq. $(15)_1$ for n or Eq. (18) for a_i to close the system (the S_1 balance equation is not useful in this context).

At the end, the break-up and coalescence terms $B_0^{+/-}$ and $C_0^{+/-}$ must be modelled. Here we have retained the model proposed by Wu et al. (1998) for our MTLOOP calculations. This model is summarized in Appendix A.

4. First moment density approach: use of a log–normal law

In the framework of their study on the coalescence of bubbles in microgravity, Kamp and co-workers (Kamp, 1996; Kamp et al., 2001; Riou, 2003; Colin et al., 2004) developed a model in the context of Eqs. (10). They have also assumed that the bubble diameter distribution function can be adequately described by a log–normal law, which reads:

$$f(d;\underline{x},t) = \frac{n(\underline{x},t)}{\sqrt{2\pi}\hat{\sigma}(\underline{x},t)d}\exp\left[-\frac{\{\ln(d/d_{00}(\underline{x},t))\}^2}{2\hat{\sigma}(\underline{x},t)^2}\right] \quad (19)$$

where $d_{00}(\underline{x},t)$ and $\hat{\sigma}(\underline{x},t)$ are a characteristic diameter and a width parameter, respectively. The diameter d_{00} stands for the number-median diameter, the number of bubbles for which $d < d_{00}$ being the same as that for which $d > d_{00}$ (Kamp et al., 2001). Eq. (19) shows that the bubble diameter distribution function is completely determined at a point $(\underline{x},t)$ by the knowledge of the quantities $d_{00}(\underline{x},t)$, $\hat{\sigma}(\underline{x},t)$ and $n(\underline{x},t)$. The two parameters of the diameter probability density function are analytically expressed by the following functions of the particular moment densities S_1 and S_2 and of the void fraction α (Kamp et al., 2001):

$$\hat{\sigma} = \sqrt{\ln\left(\frac{6\alpha S_1}{\pi S_2^2}\right)}, \qquad d_{00} = \frac{6\alpha}{\pi S_2}e^{-5\hat{\sigma}^2/2} \quad (20)$$

Then, these two parameters being known, any moment density defined by relation (3) can be analytically expressed by the following relation:

$$S_p = \frac{6\alpha}{\pi}d_{00}^{p-3}\exp[\hat{\sigma}^2(p^2-9)/2] \quad (21)$$

In particular, we have for the bubble number density:

$$n = \frac{6\alpha}{\pi d_{00}^3}\exp[-9\hat{\sigma}^2/2] \quad (22)$$

It is worth pointing out that the deduction of the two parameters d_{00} and $\hat{\sigma}$ from a couple of two moment densities S_p and $S_{q\neq p}$ is not straightforward and not even always well mathematically defined. Nevertheless one has been able to deduce these parameters from S_1 and S_2 while ensuring conservation of a_i and positivity of $\hat{\sigma}$. In this way, the system is completely closed by the resolution of the two balance equations for S_1 and S_2 given by Eqs. (10). Making similar assumptions as in Section 3 for the gas compressibility terms, these equations read:

$$\begin{aligned}\frac{\partial S_1}{\partial t} + \nabla.(S_1\underline{V}_G) &= -\nabla.[(S_1(\underline{V}_1 - \underline{V}_G))] - \frac{S_1}{3\rho_G}\left(\frac{\partial \rho_G}{\partial t} + \underline{V}_G.\nabla\rho_G\right) \\ &\quad + B_1^+ - B_1^- + C_1^+ - C_1^- \\ \frac{\partial S_2}{\partial t} + \nabla.(S_2\underline{V}_G) &= -\nabla.[(S_2(\underline{V}_2 - \underline{V}_G))] - \frac{2S_2}{3\rho_G}\left(\frac{\partial \rho_G}{\partial t} + \underline{V}_G.\nabla\rho_G\right) \\ &\quad + B_2^+ - B_2^- + C_2^+ - C_2^-\end{aligned} \quad (23)$$

In the original model of Kamp, the coalescence terms $C_1^{+/-}$ and $C_2^{+/-}$ were the only terms which were taken into account in the RHS of Eqs. (23). The modelling of these coalescence terms is given in Appendix A.

In the following, we give some general comments on the other terms.

The second term in the RHS of each balance equation (23) represents the effect of the gas compressibility onto the moment densities S_1 and S_2 and needs no further modelling.

The first terms in the RHS of Eqs. (23) are clearly an effect of the multiple sizes of bubbles, as it can be seen from the definition $(9)_1$. In his modelling of multi-size droplet flows, Mossa (2005) also adopts a log–normal law for the droplet diameter distribution function, and a Gaussian law to model the droplet velocity distribution function. In this way, this author proposes a modelling of the first terms in the RHS of Eqs. (23) which he called "uncorrelated fluxes". Unfortunately, his work on gas-droplet flows cannot be transposed to bubbly flows, because the assumption of heavier fluid particles than the continuous phase, which is true for droplets in a gas, but is false for bubbles in liquid. At this time, we have no available model for the uncorrelated fluxes, therefore these terms are neglected in our first approach, hence making a similar assumption on velocities that it was done in Section 3.

The last terms $B_1^{+/-}$ and $B_2^{+/-}$ are the break-up terms. Unfortunately, the bubble break-up contribution cannot be modelled using the present formalism with the log–normal law. The reason is that this law has a semi-infinite support, and this leads to the divergence of integrals of the break-up modelling (Riou, 2003). It seems that the only solution to alleviate this problem is to choose another mathematical expression for the bubble diameter distribution function. This will be done in the following section. Therefore, the break-up is not taken into account in the balance equations obtained in the framework of the moment density method considering a log–normal law. Eqs. (23) finally reduce to:

$$\begin{aligned}\frac{\partial S_1}{\partial t} + \nabla.(S_1\underline{V}_G) &= -\frac{S_1}{3\rho_G}\left(\frac{\partial \rho_G}{\partial t} + \underline{V}_G.\nabla\rho_G\right) + C_1^+ - C_1^- \\ \frac{\partial S_2}{\partial t} + \nabla.(S_2\underline{V}_G) &= -\frac{2S_2}{3\rho_G}\left(\frac{\partial \rho_G}{\partial t} + \underline{V}_G.\nabla\rho_G\right) + C_2^+ - C_2^-\end{aligned} \quad (24)$$

5. Second moment density approach: use of a quadratic law

Ruyer and co-workers (Ruyer, 2008; Ruyer et al., 2007; Seiler and Ruyer, 2008) chose a mathematical expression for the bubble diameter distribution function which is simpler than the log–normal law. The chosen expression is simply a second order polynomial of the variable d and is given by:

$$f(d;\underline{x},t) = \begin{cases} n(\underline{x},t)\frac{3d}{4d_{10}^3}(2d_{10}(\underline{x},t) - d) & \text{if } d \le 2d_{10} \\ 0 & \text{elsewhere} \end{cases} \quad (25)$$

The graph of the function f versus d is simply a parabola extending from the point (0,0) to the point $(2d_{10},0)$. The symmetry axis of the parabola is a vertical line which cuts, on one hand, the axis d at

the particular diameter d_{10}, and on the other hand, cuts the curve at its maximum. Therefore, the maximum of f is obtained for the diameter d_{10}, which is also the number-median diameter. The p th-order moment of the distribution function (25) is obtained analytically as:

$$S_p = \frac{6n(2d_{10})^p}{(p+2)(p+3)} \tag{26}$$

In particular, the following relations between the averaged geometrical quantities are obtained:

$$n = \frac{1}{24.3\pi}\frac{a_i^3}{\alpha^2}, \qquad d_{10} = \frac{9}{2}\frac{\alpha}{a_i}, \qquad d_{32} = \frac{4}{3}d_{10} \tag{27}$$

As n and d_{10} both are expressed as functions of α and a_i, the knowledge of these last two quantities is sufficient to completely close the system based on the distribution function (25). Therefore, the authors chose to solve the balance equation for the IAC given by Eq. $(15)_3$ with particular expressions of the coalescence and break-up terms deduced from (25) combined with chosen expressions for the coalescence and break-up kernels. Their coalescence and break-up models are summarized in Appendix A. They do not consider a different velocity to transport a_i than the mean gas velocity (i.e. they made the assumption $\underline{V}_2 = \underline{V}_G$) but they obtained averaged expressions for the drag and lift coefficient, using (25) considering the drag coefficient model given by Ishii (1990) and the lift coefficient established by Tomiyama (1998). This approach based on the moment density method and such quadratic bubble diameter distribution function has already been adapted to boiling bubbly flow studies.

6. Multi-field approach

The so-called MUSIG model (for Multi-Size-Group), sometimes called the multi-field or multi-class approach (Oesterlé, 2006), is probably the most popular method to calculate bubbly flows with bubble multiple sizes (Tomiyama and Shimada, 1998; Carrica et al., 1999; Lucas et al., 2001; Jones et al., 2003; Chen et al., 2005; Krepper et al., 2006; Sha et al., 2006; Lucas and Krepper, 2007). This method consists in deciding of a minimal and a maximal values for the bubble diameter $d_{\min}$ and $d_{\max}$ (i.e. an interval $[d_{\min}, d_{\max}]$ within the different bubble diameters lie) and to split this interval into N sub-intervals $[d_{i-1/2}, d_{i+1/2}]$, each sub-interval being centred on a discrete value of the bubble diameter d_i. The ith class, or field, is defined as the set of bubbles having their diameter comprised between $d_{i-1/2}$ and $d_{i+1/2}$.

The bubble number density of the bubbles in class i is defined as:

$$n_i \hat{=} \int_{d_{i-1/2}}^{d_{i+1/2}} f(d;\underline{x},t)\delta d \tag{28}$$

and the mean volumetric fraction (void fraction) related to the same class α_i is defined as:

$$\alpha_i \hat{=} \int_{d_{i-1/2}}^{d_{i+1/2}} \frac{\pi d^3}{6} f(d;\underline{x},t)\delta d \cong n_i \frac{\pi d_i^3}{6} \tag{29}$$

The discrete diameters d_i being known (they are chosen by the code user at the beginning of the calculation and are assumed constants during all the calculation), it is equivalent to solve the problem considering variables such as the bubble number densities n_i or the partial void fractions α_i. The averaged gas density and velocity for the bubbles in the ith class are defined by the following relations:

$$\begin{aligned} \alpha_i\rho_{g,i} &\hat{=} \int_{d_{i-1/2}}^{d_{i+1/2}} \rho(d;\underline{x},t)\tfrac{\pi d^3}{6} f(d;\underline{x},t)\delta d \\ \alpha_i\rho_{g,i}\underline{V}_{g,i} &\hat{=} \int_{d_{i-1/2}}^{d_{i+1/2}} \rho(d;\underline{x},t)\underline{v}(d;\underline{x},t)\tfrac{\pi d^3}{6} f(d;\underline{x},t)\delta d \end{aligned} \tag{30}$$

In the case of isothermal flows considered here, the multi-field approach consists in solving $2N$ mass and momentum balance equations for the N different gas fields corresponding to the N sizes, together with the two mass and momentum balance equations for the liquid phase. As the diameters are known and remain at constant values for all the bubble classes, the resolution of interfacial area balance equations is not necessary. This should be necessary in a (more complicated) variant of the method where the bubble diameters would vary in time and space. Here, the bubble coalescence, bubble break-up and gas compressibility phenomena imply mass (and possibly momentum) exchange terms between the different bubble classes. In what follows, we derive the mass balance equation for the general bubble class i.

The mass balance equation for the bubbles in the ith class is obtained by multiplying the Liouville–Boltzmann equation (7) by the bubble mass $\rho\pi d^3/6$ and integrating the resulting equation between $d_{i-1/2}$ and $d_{i+1/2}$. In order to do that, it is assumed that the gas density does not depend on the considered class, i.e. on the bubble diameter. The integration of the first two terms gives:

$$\begin{aligned} &\int_{d_{i-1/2}}^{d_{i+1/2}} \rho\tfrac{\pi d^3}{6}\tfrac{\partial f}{\partial t}\delta d = \tfrac{\partial \alpha_i\rho_g}{\partial t} - \int_{d_{i-1/2}}^{d_{i+1/2}} f\tfrac{\pi d^3}{6}\tfrac{\partial \rho}{\partial t}\delta d \\ &\int_{d_{i-1/2}}^{d_{i+1/2}} \rho\tfrac{\pi d^3}{6}\nabla.(f\underline{v}(d;\underline{x},t))\delta d = \nabla.(\alpha_i\rho_g\underline{V}_{g,i}) - \int_{d_{i-1/2}}^{d_{i+1/2}} f\tfrac{\pi d^3}{6}\underline{v}.\nabla\rho\delta d \end{aligned} \tag{31}$$

Integrating by parts the third term in the LHS of (7), we find:

$$\begin{aligned} \int_{d_{i-1/2}}^{d_{i+1/2}} \rho\frac{\pi d^3}{6}\frac{\partial fG(d;\underline{x},t)}{\partial d}\delta d &= \rho_G\frac{\pi d_{i+1/2}^3}{6}f(d_{i+1/2})G(d_{i+1/2}) \\ &\quad - \rho_G\frac{\pi d_{i-1/2}^3}{6}f(d_{i-1/2})G(d_{i-1/2}) \\ &\quad - \int_{d_{i-1/2}}^{d_{i+1/2}} \rho\frac{\pi d^2}{2}fG(d;\underline{x},t)\delta d \end{aligned} \tag{32}$$

As shown by Eq. (13), the bubble growth rate G, due to compressibility, is approximately given by $-(d/3\rho)(\partial\rho/\partial t + \underline{v}.\partial\rho)$. Substituting this expression for G into the last term in the RHS of Eq. (32) and adding the resulting equation to Eq. (31), we obtain:

$$\begin{aligned} &\int_{d_{i-1/2}}^{d_{i+1/2}} \rho\frac{\pi d^3}{6}\left(\frac{\partial f}{\partial t} + \nabla.(f\underline{v}) + \frac{\partial fG}{\partial d}\right)\delta d \\ &= \frac{\partial \alpha_i\rho_g}{\partial t} + \nabla.(\alpha_i\rho_g\underline{V}_{g,i}) + \rho_G\frac{\pi d_{i+1/2}^3}{6}f(d_{i+1/2})G(d_{i+1/2}) \\ &\quad - \rho_G\frac{\pi d_{i-1/2}^3}{6}f(d_{i-1/2})G(d_{i-1/2}) \end{aligned} \tag{33}$$

Finally, the integration of the complete equation (7) gives the following mass balance equation for the ith class:

$$\begin{aligned} \frac{\partial \alpha_i\rho_g}{\partial t} + \nabla.(\alpha_i\rho_g\underline{V}_{g,i}) &= \rho_G\frac{\pi d_{i-1/2}^3}{6}f(d_{i-1/2})G(d_{i-1/2}) \\ &\quad - \rho_G\frac{\pi d_{i+1/2}^3}{6}f(d_{i+1/2})G(d_{i+1/2}) \\ &\quad + B_i^+ - B_i^- + C_i^+ - C_i^- \end{aligned} \tag{34}$$

with the following definition for the term B_i^+:

$$B_i^+(\underline{x},t) \hat{=} \int_{d_{i-1/2}}^{d_{i+1/2}} \rho\frac{\pi d^3}{6}B^+(d;\underline{x},t)\delta d \tag{35}$$

and similar definitions for B_i^-, C_i^+ and C_i^-. The description of these break-up and coalescence terms is given in Appendix A. The first two terms in the RHS of Eq. (34) represent the mass fluxes entering into the bubble class i and exiting from it. These fluxes are due to the bubbles size growth or reduction caused by gas density variations. Before deriving an approximate closed expression for these

fluxes, we must establish the conditions that should be verified by the total gas mass balance equation. This equation is obtained by summing the N equations (34) written for the N classes regarding that:

$$\alpha = \sum_{i=1}^{N} \alpha_i, \qquad \alpha \underline{V}_g = \sum_{i=1}^{N} \alpha_i \underline{V}_{g,i} \tag{36}$$

The first relation (36) simply recalls that the total void fraction is the sum of the partial void fractions of the N classes, and the second one defines the mean gas velocity as the velocity of the centre of volume of all the bubbles (which coincides with the centre of mass when the gas density does not depend on the bubble size, as it is assumed here). The obtained total gas mass balance equation reads:

$$\begin{aligned} &\frac{\partial \alpha \rho_g}{\partial t} + \nabla.(\alpha \rho_g \underline{V}_g) \\ &\quad = -\rho_g \sum_{i=1}^{N} \left[\frac{\pi d_{i+1/2}^3}{6} f(d_{i+1/2}) G(d_{i+1/2}) - \frac{\pi d_{i-1/2}^3}{6} f(d_{i-1/2}) G(d_{i-1/2}) \right] \\ &\quad = -\rho_g \left[\frac{\pi d_{N+1/2}^3}{6} f(d_{N+1/2}) G(d_{N+1/2}) - \frac{\pi d_{1/2}^3}{6} f(d_{1/2}) G(d_{1/2}) \right] \end{aligned} \tag{37}$$

considering that the coalescence and break-up phenomena do not change the total amount of gas (Appendix A.4). The following boundary conditions on G are derived from the identification of Eq. (37) with Eq. $(1)_1$ for $k = g$:

$$G(d_{1/2}) = G(d_{N+1/2}) = 0 \tag{38}$$

Conditions (38) have no physical basis, and are even incoherent with Eq. (13). Nevertheless, they are coherent with the method described here which considers only bubble diameters between $d_{\min} = d_{1/2}$ and $d_{\max} = d_{N+1/2}$. As it is assumed with this method that no gas is present for bubble diameters smaller than $d_{1/2}$ or greater than $d_{N+1/2}$, conditions (38) are simply boundary conditions on G which guarantee that the gas cannot exit from the authorized bubble diameter range. Now we must establish approximate expressions for the first two terms in the RHS of Eq. (34). When the index $i + 1/2$ is different from ½ or $N + 1/2$, the growth rate G is calculated as an approximate form of Eq. (13):

$$\begin{aligned} &G(d_{i+1/2}) = -\tfrac{d_{i+1/2}}{3\rho_g} \left(\tfrac{\partial \rho_g}{\partial t} + \underline{V}_{g,i+1/2}.\nabla \rho_g \right) \quad \text{with :} \\ &d_{i+1/2} = \tfrac{d_i + d_{i+1}}{2} \quad \text{and} \quad \underline{V}_{g,i+1/2} = \tfrac{\underline{V}_{g,i} + \underline{V}_{g,i+1}}{2} \end{aligned} \tag{39}$$

The distribution function at the diameter $d_{i+1/2}$ is calculated by using the following approximation:

$$\begin{aligned} &\int_{d_i}^{d_{i+1}} \frac{\pi d^3}{6} f(d) \delta d \cong \frac{\pi d_{i+1/2}^3}{6} f(d_{i+1/2})[d_{i+1} - d_i] \hat{=} \alpha_{i+1/2} \\ &\qquad \Rightarrow \frac{\pi d_{i+1/2}^3}{6} f(d_{i+1/2}) = \frac{\alpha_{i+1/2}}{[d_{i+1} - d_i]} \end{aligned} \tag{40}$$

In order to evaluate the value of $\alpha_{i+1/2}$, we use an upwind scheme according to the sign of the function G:

$$\alpha_{i+1/2} G(d_{i+1/2}) = \alpha_i \max(G(d_{i+1/2}), 0) + \alpha_{i+1} \min(G(d_{i+1/2}), 0) \tag{41}$$

Finally, the mass balance equation (34) for the bubble class i can be rewritten as:

$$\begin{aligned} \frac{\partial \alpha_i \rho_g}{\partial t} + \nabla.(\alpha_i \rho_g \underline{V}_{g,i}) = {} & \rho_G \frac{\alpha_{i-1/2}}{[d_i - d_{i-1}]} G(d_{i-1/2}) - \rho_G \frac{\alpha_{i+1/2}}{[d_{i+1} - d_i]} G(d_{i+1/2}) \\ & + B_i^+ - B_i^- + C_i^+ - C_i^- \end{aligned} \tag{42}$$

with the four terms B_i^+, B_i^-, C_i^+ and C_i^- given in Appendix A.

In the present state of the method, we do not take into account the bubble momentum transfers between classes, due to the different mass transfers appearing in the RHS of Eq. (42). It is assumed that these transfers are negligible in comparison to the interfacial momentum transfers between each bubble class and the liquid phase. Neglecting the momentum transfers associated to the mass transfers, the momentum equation $(1)_2$ continues to be valid but we have now N equations $(1)_2$ for the N gas fields. Each of these equations involves an interfacial transfer term $\underline{M}_{g,i}$ which is the sum of a drag force, an added mass force, a lift force...acting on bubbles of diameter d_i. The momentum interfacial transfer in the liquid phase $\underline{M}_L$ is consequently the sum of the N terms $\underline{M}_{g,i}$ with the opposite sign, in order to verify Eq. (2). The various averaged forces being calculated according to the appropriate values of the diameter and of the partial void fraction of each class, they will differ from one class to another one. Therefore, the bubbles of the different classes will have different mean velocities, in magnitude and in direction. So it is worthwhile to underline that this approach takes into account in a natural way the multiple velocities associated with the multiple sizes, a characteristic that is not easily handled by other approaches presented in the preceding sections.

7. Description of the MTLOOP experiment

In the MTLOOP facility (Lucas et al., 2005), the evolution of a two-phase bubbly flow is observed in a vertical tube having an inner diameter equal to 51.2 mm and a length equal to 3.5 m. An air–water mixture at a temperature equal to 30 °C is supplied at the bottom of the tube. The use of a wire-mesh sensor allows to measure radial profiles of void fraction for a given range of bubble sizes, as well as bubble size distribution functions. The measurements are performed for up to 10 different inlet lengths and for about 100 combinations of gas and liquid volume flow rates. Here we choose to simulate the test number 118 which is characterized by a liquid inlet superficial velocity J_L equal to 1.017 m/s and a gas inlet superficial velocity J_G equal to 0.219 m/s.

The distance between the wire-mesh sensor and the air injection device varies from 0.03 m to 3.03 m (inlet lengths 0.6–60 L/D). Ten axial distances are investigated, corresponding to 10 measuring sections, each identified by a letter. The correspondence between the measuring sections and the distances from the air injection device is given in Table 1.

Data are recorded by an electrode wire-mesh sensor that measures the instantaneous conductivity distribution. The conductivity is a measurement from which is derived the gas volume fraction. The spatial resolution is given by the pitch of the electrode wires which is equal to 2 mm. The number of electrode wires is $24 * 24$. A number of 2500 cross-sectional frames per second is recorded, during a measuring time equal to 10 s. Therefore, the matrix of the measurement for each measuring section has the dimension of $24 * 24 * 25{,}000$.

A special procedure allows the identification of single bubbles and the determination of their volume v, and hence, of their volume-equivalent diameter:

$$d = \sqrt[3]{\frac{6v}{\pi}} \tag{43}$$

Using this procedure, bubble size distributions as well as gas volume fraction profiles for bubbles within a predefined interval

Table 1
Distances between the 10 measuring sections and the air injection device.

Section	A	B	C	D	E	F	H	J	K	L
Z (m)	0.03	0.08	0.13	0.23	0.43	0.83	1.53	2.03	2.53	3.03

of bubble sizes can be evaluated. For the calculation of bubble size distributions, the equivalent bubble diameter is subdivided into intervals and the contribution of each individual bubble to the gas volume fraction is evaluated for each interval. This gives bubble size distribution functions related to the gas volume fraction instead of being related to the bubble number density (f). The latter has the disadvantage of poorly reflecting the number of large bubbles, since the number density of small bubbles is much higher. According to this new definition of the bubble size distribution function:

$$h(d) \hat{=} \frac{\delta\alpha}{\delta d} \tag{44}$$

the integral over all possible bubble sizes results in the total void fraction:

$$\alpha = \int_0^\infty h(d)\delta d \tag{45}$$

In each measuring section, we dispose of the radial profile of the total void fraction defined by Eq. (45) and the bubble diameter distribution function defined by Eq. (44) averaged over the duct cross-section. These quantities will be compared to the numerical results obtained with the help of the NEPTUNE_CFD code considering the various approaches into the following section.

8. Numerical simulations of the MTLOOP experiment

All the numerical simulations presented in this section have been performed with the NEPTUNE_CFD code, developed jointly by Electricité de France and the French Commissariat à l'Energie Atomique, these developments being also financially supported by AREVA_NP and the Institut de Radioprotection et de Sûreté Nucléaire. This code is based on the two-fluid approach (Eqs. (1)) generalized into an N-field approach (a field being defined by one set of mass, momentum and energy balance equations). Several auxiliary balance equations can be used like a two-phase K–ε model for bubbly flow (Morel, 1995; Morel et al., 2004, 2005) or additional balance equations for geometrical quantities like the ones developed in Section 2. Since we are dealing with isothermal flows without phase change, it is sufficient to solve the mass and momentum balance equations (1) (the enthalpy equations are not solved) together with the K–ε model for the liquid phase and the geometrical balance equation(s) for the gas phase. The description of the K–ε model is postponed to Appendix B.

8.1. Single-size bubble approach

In this approach, we use the single-size model as derived by Wu et al. (1998). We solve the bubble number density balance equation $(15)_1$ together with the coalescence and break-up terms given by Eqs. (A.1)–(A.4) in Appendix A. The momentum interfacial transfer term $\underline{M}_k$ is assumed to be the sum of five forces: the drag force, the added mass force, the lift force, the turbulent dispersion force and the wall force. In the following, we give the detailed expressions of these forces. The drag force is classically expressed by the following expression:

$$\underline{M}_G^D = -\underline{M}_L^D = -\frac{1}{8}a_i\rho_L C_D|\underline{V}_G - \underline{V}_L|(\underline{V}_G - \underline{V}_L) \tag{46}$$

The drag coefficient C_D has been empirically modelled by Ishii (1990):

$$\begin{aligned} &C_D = \tfrac{2}{3}d\sqrt{\tfrac{g|\rho_G-\rho_L|}{\sigma}}\left\{\tfrac{1+17.67|f(\alpha)|^{6/7}}{18.67f(\alpha)}\right\} \quad \text{with} f(\alpha) = (1-\alpha)^{1.5} \quad \text{distorted bubbles} \\ &C_D = \tfrac{8}{3}(1-\alpha)^2 \quad \text{churn-turbulent regime} \end{aligned} \tag{47}$$

According to the value of the diameter d, the bubbles fall into the distorted bubble regime or into the churn-turbulent regime.

The added mass force is given by the following expression:

$$\underline{M}_G^A = -\underline{M}_L^A = -C_A E(\alpha)\alpha\rho_L\left[\left(\frac{\partial\underline{V}_G}{\partial t} + \underline{V}_G.\underline{\underline{\nabla}}\underline{V}_G\right) - \left(\frac{\partial\underline{V}_L}{\partial t} + \underline{V}_L.\underline{\underline{\nabla}}\underline{V}_L\right)\right] \tag{48}$$

The added mass coefficient C_A for a single spherical bubble is equal to 0.5, but due to the presence of the other bubbles, Zuber (1964) proposed to correct this value by the factor $E(\alpha) = (1 + 2\alpha)/(1-\alpha)$, on the basis of a calculation performed by Lamb (1932).

The lift force is given by the following relation (Auton, 1987):

$$\underline{M}_G^L = -\underline{M}_L^L = -C_L\alpha\rho_L(\underline{V}_G - \underline{V}_L)\wedge(\underline{\nabla}\wedge\underline{V}_L) \tag{49}$$

The lift coefficient C_L is given by the following empirical correlation (Tomiyama, 1998):

$$C_L = \begin{cases} \min\begin{bmatrix} 0.288\tanh(0.121\mathrm{Re}), \\ 0.00105\mathrm{Eo}_H^3 - 0.0159\mathrm{Eo}_H^2 - 0.0204\mathrm{Eo}_H + 0.474 \end{bmatrix} & \text{if } \mathrm{Eo}_H < 4 \\ 0.00105\mathrm{Eo}_H^3 - 0.0159\mathrm{Eo}_H^2 - 0.0204\mathrm{Eo}_H + 0.474 & \text{if } 4 \le \mathrm{Eo}_H \le 10 \\ -0.27 & \text{if } \mathrm{Eo}_H > 10 \end{cases} \tag{50}$$

with the modified Eotvos number defined by:

$$\mathrm{Eo}_H \hat{=} \frac{g(\rho_L - \rho_G)d_H^2}{\sigma} \tag{51}$$

where d_H is the maximum horizontal dimension of the deformed bubble, which is calculated using an empirical correlation given by Wellek et al. (1966), as reported by Krepper et al. (2006):

$$d_H = d\sqrt[3]{1 + 0.163\mathrm{Eo}^{0.757}} \tag{52}$$

where d is the (spherical) equivalent bubble diameter and Eo has a similar expression as Eq. (51) with d instead of d_H. The bubble Reynolds number Re is calculated according to the classical definition.

The turbulent dispersion force is modelled according to Krepper et al. (2006) and is given by the following expression:

$$\underline{M}_G^{TD} = -\underline{M}_L^{TD} = -\frac{3}{4}\frac{C_D}{d}\rho_L v_L^T|\underline{V}_G - \underline{V}_L|\nabla\alpha \tag{53}$$

where C_D is the drag coefficient and v_L^T is the liquid turbulent viscosity, which is obtained from the solution of the K–ε model.

The wall force is the one derived by Antal et al. (1991). It reads:

$$\begin{aligned} &\underline{M}_G^W = -\underline{M}_L^W = \frac{\alpha\rho_L}{R_b}|U_{//}|^2\max\left[0, C_{W1} + C_{W2}\frac{R_b}{y}\right]\underline{n}_W \\ &\underline{U}_{//} = (\underline{V}_G - \underline{V}_L) - [(\underline{V}_G - \underline{V}_L).\underline{n}_W]\underline{n}_W \\ &C_{W1} = -0.104 - 0.06U_R \\ &C_{W2} = 0.147 \end{aligned} \tag{54}$$

where $R_b = d/2$ is the bubble radius, y is the distance to the wall, $\underline{n}_W$ is the unit vector normal to the wall surface and $\underline{U}_{//}$ is the tangential part of the relative velocity, U_R being its norm.

For the two moment methods, as well as for the single-size model, all the forces presented above are calculated by using the bubble Sauter mean diameter d_{32}, which is always available. For the multi-field method, each bubble class is characterized by a single bubble diameter d_i and a corresponding momentum balance. The momentum exchanges between this particular gas field and the continuous liquid field are also calculated with the models given in Eqs. (46)–(54) with the corresponding value of the bubble diameter d_i.

Due to the sensitivity of our results to the lift model, we have plotted the curve representing the lift coefficient given by Eq. (50)

for an air–water system at normal conditions (Supplementary Fig. S1). It can be seen that the sign of the lift coefficient changes for a bubble diameter approximately equal to 5.8 mm.

Three different grids have been used to calculate the MTLOOP experiment, named mtloop1,2 or 3, respectively. As the flow remains axi-symmetric, the grids are reduced to two-dimensional regular grids of the plane (r,z). The basic grid mtloop1 consists in 10 radial meshes and 100 axial meshes. The two other grids are obtained from the first one by multiplying the number of meshes in each direction by a factor 2, therefore the second grid mtloop2 has 20 radial meshes and 200 axial meshes and the third one, mtloop3, has 40 radial meshes and 400 axial meshes. We have first made three calculations with Wu's model on these three grids to test the grid sensitivity. The grid convergence is nearly attained with the second grid, mtloop2, since the results do not change significantly between the second grid and the third one. This is illustrated in a comparison of the void fraction profiles taken in Section L (Supplementary Fig. S2).

In Fig. 1, we compare the results obtained with the finest grid and the experimental total void fraction (Eq. (45)) for the 10 radial profiles. The 10 different pictures in this figure correspond to the different measuring sections indicated in Table 1. In each of these pictures, the experimental profile is indicated by red circles and the calculated one is indicated by a black continuous line. It can be seen in Fig. 1 that the experimental profile near the inlet is not flat.

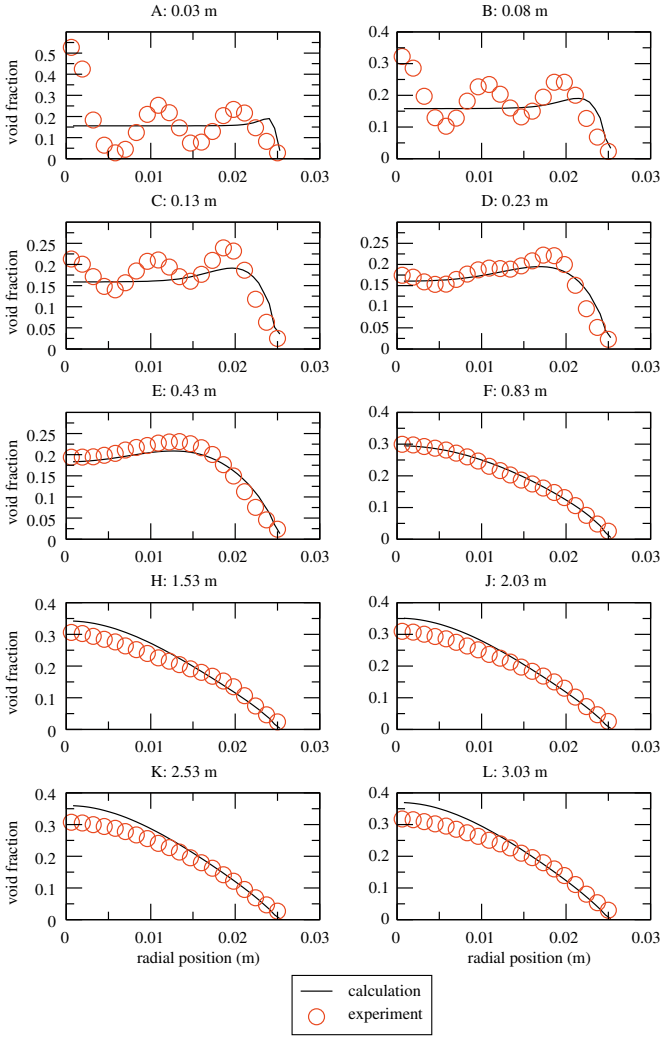

Fig. 1. Void fraction. Single-size approach.

It would be possible to reproduce such inlet conditions for the single-size approach but one of our final goals is to compare all the approaches in the same conditions.

Unfortunately, we had not enough information to reproduce this profile in our calculations in the approach considering several groups of bubbles (the multi-field method) since we dispose only of the radial profiles of the *total* void fraction and the bubble diameter distribution function *averaged over the duct cross-section* (see Section 7). Therefore, we are not able to reproduce the inlet conditions for each partial void fraction field in the multi-field method (see Section 8.4) for each point of the radial profile. That is why we choose to ignore the inlet shape of the void fraction profile whatever the approach is. So, flat profiles are imposed, which conserve the averaged values of the void fraction as well as the liquid and gas superficial velocities. Fortunately, as it can be seen in Fig. 1, the influence of the inlet shape rapidly disappears along the flow because of bubbles radial migration. From the fourth measuring Section D up to the last one L, the simulation results obtained on the void fraction profiles are in quite good agreement with the data. In particular, the so-called "void coring" (a maximum of the void fraction in the central part of the tube) observed in the experiment is reproduced.

As the experimental bubble diameter distribution function defined by Eq. (44) is available in each measuring section, we can deduce from it the different mean diameters defined by Eq. (4) and the different moment densities defined by Eq. (5). According to the particular definition (44), these quantities read:

$$d_{10} = \frac{\int dh(d)\delta d}{\int h(d)\delta d}, \quad d_{20} = \left(\frac{\int d^2 h(d)\delta d}{\int h(d)\delta d}\right)^{1/2}, \quad d_{30} = \left(\frac{\int d^3 h(d)\delta d}{\int h(d)\delta d}\right)^{1/3},$$
$$d_{32} = \frac{\int d^3 h(d)\delta d}{\int d^2 h(d)\delta d} \qquad (55)$$
$$n = S_0 = \frac{6\alpha}{\pi d_{30}^3}, \quad a_i = \pi S_2 = n\pi d_{20}^2$$

Relations (55) lead to one value of each quantity in each measuring section, since $h(d)$ is a global quantity defined in each measuring section. So, in order to compare our results to the experimental quantities defined by Eqs. (55), we should proceed to their spatial averages over the duct cross-section. We make such an operation for the two quantities considered in Wu's model: the interfacial area concentration a_i and the bubble Sauter mean diameter d_{32}. The comparison of the axial profiles (taken along the tube) of the spatially averaged quantities $\langle a_i \rangle$ and $\langle d_{32} \rangle$ are illustrated in Supplementary Figs. S3 and S4, and also in Figs. 5 and 6 which give the comparison between the different approaches.

It can be seen in these figures that the IAC and the SMD are quite well reproduced in the first half of the tube (up to z = 1.53 m). In the second half, the IAC is overestimated and the SMD is underestimated by Wu's model. The calculated SMD is always greater than 6 mm, therefore the lift coefficient remains negative, as it can be seen in Supplementary Fig. S1. Thus, the lift force is directed towards the pipe axis, which could explain the formation of the void coring.

8.2. Moments approach based on the log–normal law

In this subsection, the results obtained by using the model presented in Section 4 are presented. The partial differential equations solved for the bubbles geometry are the two equations (24) with the coalescence terms given in Eqs. (A.5) in Appendix A. It can be seen from (A.5) that the coalescence terms C_1 and C_2 are proportional to an adjustable constant K_C which was fitted equal to 1 by the authors of the original model (Kamp et al., 2001). We first made some calculations with this value, but it did not manage to

produce the large experimental level of bubble coalescence. Some sensitivity calculations to the value of K_C have thus been made, and the value $K_C = 50$ has been retained for the calculations presented here. About the forces influencing the interfacial momentum transfer, the models are the same than those presented in Section 8.1. The diameter used to evaluate these forces is the Sauter mean diameter d_{32}, as it was the case in the previous subsection. The three different grids mtloop1,2,3 have also been tested. The grid convergence is attained without difficulty and we present here the results obtained with the finest grid.

The results are presented in Supplementary Figs. S5–S7 except Fig. 2. The notation dalpha/dd in Fig. 2 corresponding to $h(d)$ defined in Eq. (44).

The comparisons presented in Supplementary Fig. S5 and Fig. 1 show that there is very little change on the prediction of the axial evolution of the radial void fraction profile compared to the previous approach. This is essentially due to the lift force because the major part of the bubbles has their diameters (Fig. 2 and Supplementary Fig. S7) greater than the critical diameter (approximately 6 mm) for which the sign of the lift force changes. Nevertheless, the lift force being essentially directed toward the pipe centre (negative lift coefficient), a void coring rapidly takes place, as it was the case in the calculation with the single-size approach. Fig. 2 gives the comparison of the axial evolution of the bubble diameter distribution function defined by Eq. (44). The red stairs curves correspond to the measured distribution functions in the 10 cross-sections, and the black line curves correspond to the log–normal law, as determined by Eqs. (19) and (20) (previously divided by n and multiplied by 100α in order to obtain $\delta\alpha/\delta d$ in %/mm). Supplementary Figs. S6 and S7 give the axial evolution of the spatially averaged IAC and of the spatially averaged SMD. These two figures clearly underline that, with the chosen value $K_C = 50$, the coalescence effect is too important in the first half of the tube, but insufficient in the second half. Fig. 2 illustrates this effect on the predicted (and experimental) distribution functions. The predicted distribution function is progressively shifted to the right, in comparison to the experimental one. The bubble size corresponding to the maximum value of the distribution function is thus too large, especially in the second half of the tube. The measured distribution function is characterized by a peak between $d = 5$ mm and 10 mm, which is the memory of the initial peak, but also by a long tail which is progressively developing for bubble diameters greater than 10 mm, up to 40 mm in the last two sections. The log–normal law is not really able to reproduce this tail, showing the limitation on the present approach based on this law.

8.3. Moments approach based on the quadratic law

The model based on the quadratic law, presented in Section 5 (Eqs. (25)–(27)) is considered. The coalescence and break-up terms

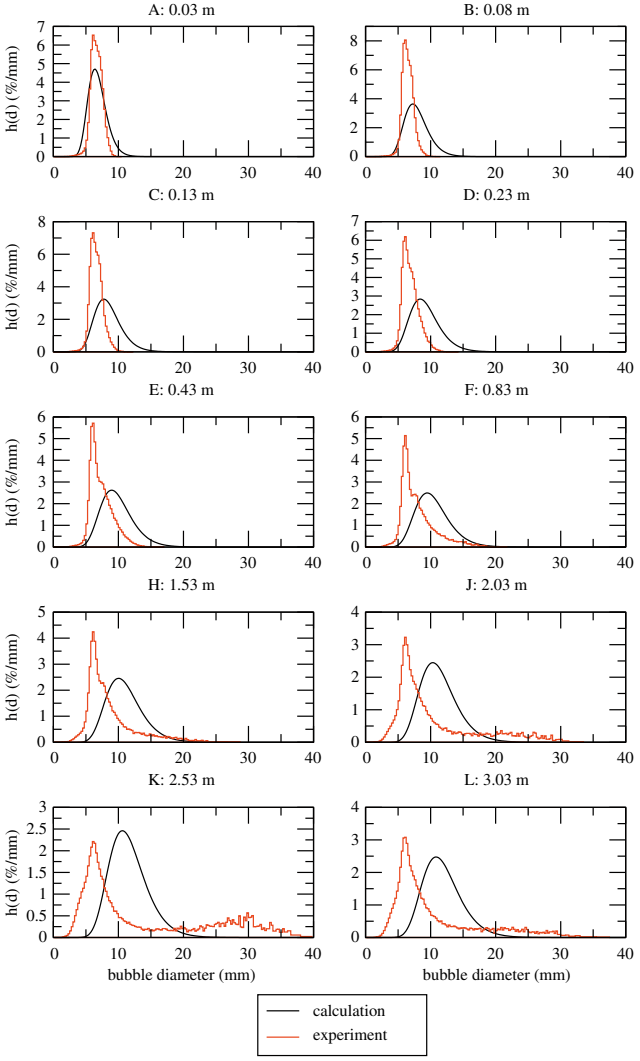

Fig. 2. Dalpha/dd (%/mm). Log–normal law.

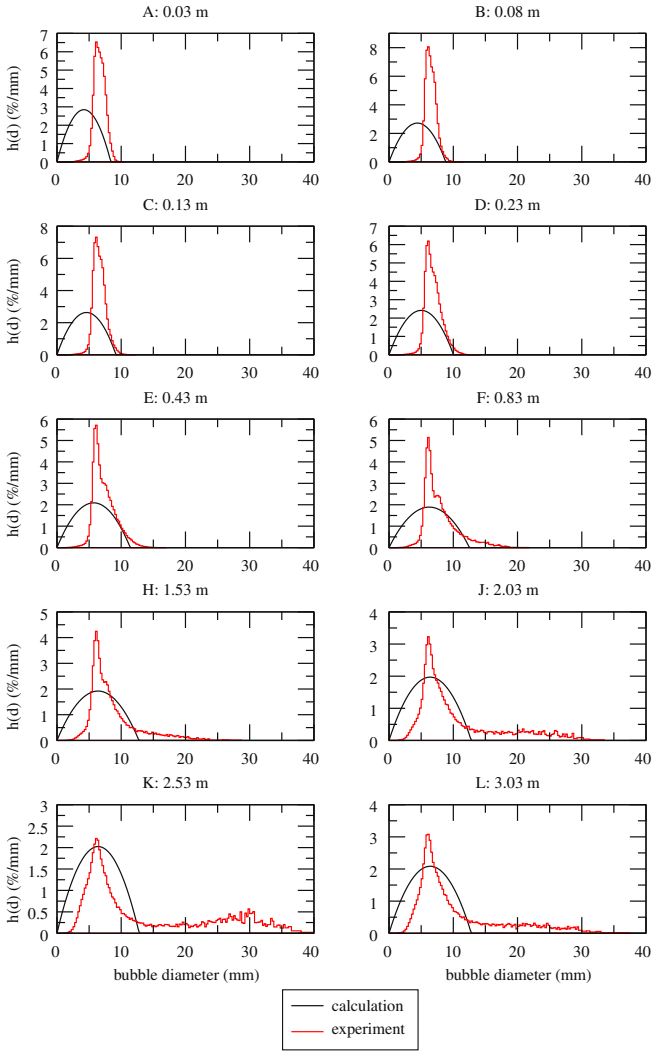

Fig. 3. Dalpha/dd (%/mm). Quadratic law.

are given by Eqs. (A.7) and (A.8) in Appendix A. The complete model gives too small sizes of bubbles (Fig. 3), but the void fraction profile predicted is quite well reproduced (Supplementary Fig. S8). Fig. 3 and Supplementary Figs. S9 and S10 show that the break-up model given by Eq. (A.8) is too strong or the coalescence model given in Eq. (A.7) is too weak. The three different grids mtloop1,2,3 have also been tested. The grid convergence is attained without difficulty and we present here the results obtained with the finest grid. A test has also been made using a different break-up model based on the model of Yao and Morel, 2004 developed for monodisperse case adapted to the quadratic law (described in Ruyer et al., 2007), but no grid convergence could be obtained. Another calculation without taking into account break-up (only coalescence) can be compared with the results obtained with the log–normal law. Corresponding results are displayed in Supplementary Figs. S9 and S10, and summarized in Figs. 5 and 6. It shows that the calculation correctly reproduced the features of the flow. Analysis of the bubble size distribution shows that the quadratic law correctly reproduced the maximum diameter of the experimental distribution. It may help to interpret the result obtained with the other calculations taking into account the break-up: break-up would be too strong rather than coalescence would be too weak.

8.4. Multi-field approach

Fig. 4 and Supplementary Figs. S11–S13 give the results obtained with the multi-field approach on the finest grid mtloop3. The grid convergence is attained without difficulty. The bubble diameter range has been chosen to cover the largest extent observed in this experimental test, namely [2 mm, 40 mm] according to the bubble diameter distribution function measured in Section L. This numerical diameter range has been subdivided into 19 bubble classes, the diameter step Δd being assumed constant. The partial void fractions imposed at the inlet for the different fields have been evaluated from the bubble diameter distribution function measured in Section A. About the interfacial momentum transfer, the models for the different forces are the same than those presented in Section 8.1, except to the fact that here they are used for each bubble field individually. The total void fraction radial profiles (Supplementary Fig. S11) are well predicted from Section D to Section L. According to Supplementary Figs. S12 and S13, the coalescence effect seems to be insufficient. However, the coalescence seems to be too important according to the axial evolution of the bubble diameter distribution function (Fig. 4). This result, associated to the results presented in the preceding paragraphs, dealing with the two other multi-size approaches, illustrate the fact that it is not necessary to reproduce correctly the bubble diameter distribution function to have the correct trend on the averaged quantities, like the IAC or the SMD, as well as on the total void fraction (at least on this particular experimental test). It is worth noting that it is possible to define several diameter distribution functions having the same IAC and total void fraction. But prediction of these average quantities does not appear to depend on the amount of information used to describe the distribution function. This surprising result can be probably due to the fact that average quantities prediction is not sensitive to additional detailed information on the distributions.

Another issue (Fig. 4) is the strong accumulation of gas near the maximum bubble diameter authorized in the calculation (40 mm) present from Section H to Section L. This is of course a numerical bias of the multi-field method based on a fixed bubble diameter range. This raises the question of the sensitivity of this method to the 'grid' adopted to describe the bubble diameter range. We can hope that this phenomenon of bubble accumulation near the maximum diameter would disappear if we simply enlarge the

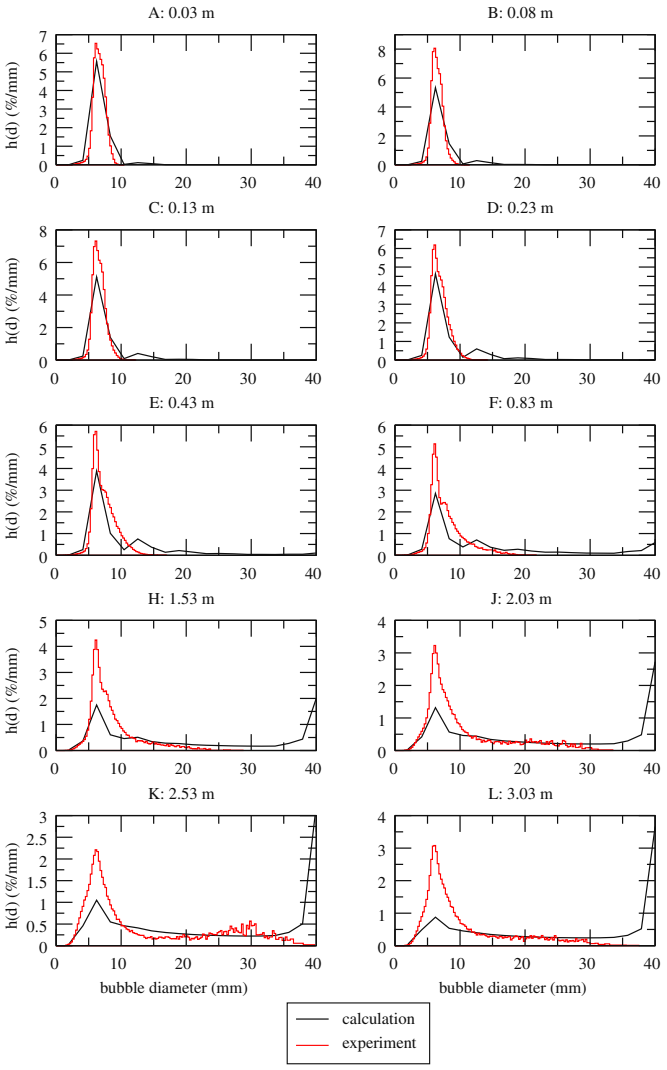

Fig. 4. Dalpha/dd (%/mm). Multi-field.

diameter range in the simulation. In our opinion, it is not so simple, because this also strongly depends on the behaviour of the coalescence model for bubbles larger than the current boundary limit of 40 mm. It seems that the convergence of this type of simulation in terms of 'bubble diameter grid' should be investigated in relation with the coalescence (and break-up in the other sense) models. It is a quite difficult (and probably long) task because of our ignorance of the physics underlying these two phenomena (coalescence and break-up) and also because of the high CPU time necessary for this kind of simulations. Except if we adopt a very simple model for the bubble diameter distribution function (like we have done in the two models based on a log–normal law and a quadratic law), the price to pay to reproduce the bubble diameter distribution function could be high (in terms of modelling efforts and of CPU time).

9. Conclusions

Four different approaches have been tested to evaluate bubble sizes in a vertical upward bubbly flow and their performances have been investigated on the MTLOOP experiment. Three of these methods handle the simultaneous existence of multiple bubble sizes. The fourth method is the classical single-size approach, where all the bubbles are characterized by a single, but variable,

diameter. The single-size approach, using one interfacial area concentration (IAC) balance equation, has been used to obtain a "reference calculation".

The major difficulty, when one considers an isothermal bubbly flow without phase change, consists in the modelling of the bubbles coalescence and break-up terms. Unfortunately, the knowledge of these two phenomena in the general situation of a large spectrum of bubble sizes, characterized by different shapes, is still insufficient to correctly predict the spatial and temporal development of such a bubbly flow in a large tube. Despite of this lack, we have used the different approaches with existing coalescence and break-up models. Our aim is not to claim that we have found the better model, or the better approach, to simulate upward bubbly flows in vertical ducts, but to compare the merits and shortcomings of the different approaches presented here. Some of these approaches, like the two variants of the moment density method presented in Sections 4 and 5, are still in their infancy, and have been used by very few people.

In the following paragraph, we will consider the different methods, and comment the obtained results on the MTLOOP experiment, approach by approach.

We have chosen the model of Wu et al. (1998) for the bubble coalescence and break-up in case of the single-size approach, because it gives quite good results on the studied experimental case. Other models have been tested like the ones from Hibiki and Ishii (2000), Ishii and Kim (2001) and also Yao and Morel (2004) but none of these models give results as good as the ones obtained with Wu's model. The strong sensitivity of the results to the model used (results not presented here) gives an idea of the importance, and also on the difficulty, to correctly model the bubble coalescence and break-up phenomena. The calculation done with Wu's model provides in a reference calculation to compare the performances of the three multi-size approaches. With this model, the cross-sectional averaged IAC and SMD axial evolutions are quite well reproduced (Figs. 5 and 6), especially in the first half of the tube. The axial evolution of the void fraction radial profile is also well reproduced (Fig. 1) showing the formation of a void coring in the second half of the tube. This void coring is attributed, at least in the model, to the negative sign of the lift coefficient when the bubble diameter is greater than a critical value of approximately 6 mm for air–water flows at ambient conditions. In fact, in all the calculations, this void coring formation is well reproduced because the predicted bubble diameters are large enough to induce a negative lift coefficient (Supplementary Fig. S1), therefore creating a lift force oriented towards the pipe axis.

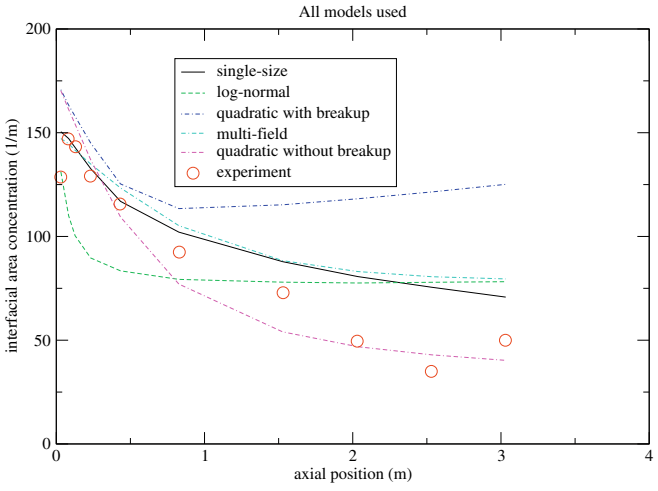

Fig. 5. Comparison of the spatial averaged IAC.

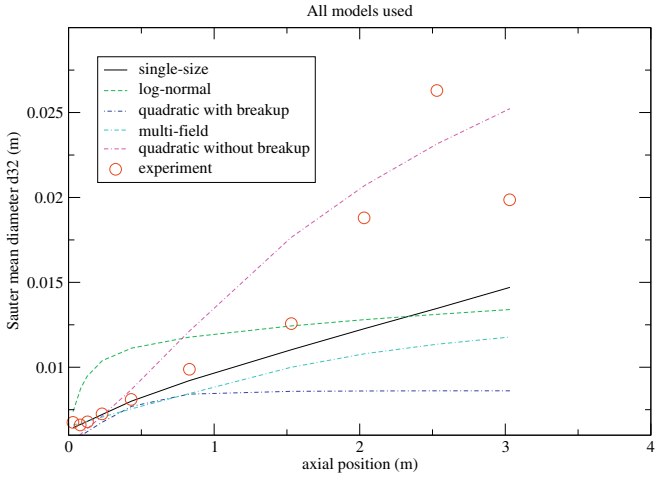

Fig. 6. Comparison of the spatial averaged Sauter mean diameter.

The first presented variant of the moment density approach is based on the log–normal law. The coalescence model previously developed by Kamp et al. (2001) in their study of bubble coalescence in microgravity has been used. The gas expansion due to compressibility is also modelled, but unfortunately we have failed to model the bubble break-up in this framework. According to Riou (2003), the break-up cannot be modelled in the context of a log–normal diameter distribution function because this law has a semi-infinite support and this makes the break-up integral in the moments equations to diverge. This is the main shortcoming of the present approach. Despite the absence of a bubble break-up term in the equations, we have been forced to strongly increase the coalescence terms (by increasing the factor K_C of the original model by 50) to obtain a sufficient coalescence effect compare to the MTLOOP experimental results. Nevertheless, considering this fitted value, the coalescence is too strong in the first half of the tube, but too weak in the second half (Figs. 5 and 6). The analysis of the log–normal distribution function compared to the experimental one (Fig. 2) shows that the log–normal law is shifted towards the big diameters, and does not reproduce the experimental tendency, but looks more alike the experimental one than the quadratic law illustrated in Fig. 3.

Indeed, the quadratic law has a parabolic shape (Fig. 3) which is far away from the shape of the distribution function experimentally observed. The bubbles break-up is overestimated in the present state of our model. Nevertheless, the void coring formation observed on the void fraction profiles is correctly reproduced. The main shortcomings of the quadratic law are (i) that its graph is symmetric with respect to the mean diameter d_{10}, which is often unrealistic because this means that we have the same quantity of small and large bubbles and that (ii) this law imposes a direct relation between the mean bubble diameter d_{10} and the width of the distribution function. Therefore the model cannot degenerate into the simple case of a unique size of bubbles, unless a nil size. These shortcomings are due to the low number of parameters in the expression (25). It could be noticed that the log–normal law has an additional parameter, in comparison to the quadratic law. This is the reason why the closure of the method based on the log–normal law needs the solution of two moment densities balance equations instead of only one for that involving the quadratic law. The great advantage of the quadratic law in comparison to the log–normal one, resides in its mathematical simplicity which allows to calculate the break-up integral, and also to properly average the drag and lift forces over the different bubble sizes. A calculation without any break-up allows to compare with the results obtained with the

log–normal law. It shows very good agreement with the experimental data and this suggests that taking into account break-up using the Wu model leads to an overestimation of the break-up.

The multi-field approach has been tested for the first time in the NEPTUNE_CFD code. This approach is completely different from the two other ones; therefore it has been presented in a detailed manner in this paper. Coalescence and break-up phenomena have been taken into account, as well as the gas expansion due to compressibility. The results obtained on the IAC measured along the tube is quite good (Supplementary Fig. S12 or Fig. 5) and the development of the void coring is also very well reproduced (Supplementary Fig. S11). The bubble diameter distribution function overlaps the experimental one at the beginning of the tube (Fig. 4) but rapidly the coalescence effect seems to be more rapid than in the experiment. This excessive simulated coalescence, together with the fixed discretisation adopted for the bubble diameter range, gives an unphysical gas accumulation near the maximum authorized diameter. Future investigations are needed on the influence of the bubble diameter range and on its discretisation, but also on the bubble coalescence and break-up mass exchange terms. It seems that this approach has more potentialities than the two previous ones (e.g. the simulation of bubbles with different sizes and different velocities comes naturally, a fact that is very difficult to model in the two other approaches). But the price to pay for this greater generality is, among others, the important calculation time needed when one uses a fine grid and an important number of different bubble sizes. Due to this difficulty, the similar MUSIG approach developed in the CFX code, groups several bubble sizes into the same velocity field, so diminishing the number of momentum equations to solve (e.g. Krepper et al., 2006).

Acknowledgements

This work was done in the frame of the NURESIM project supported by the EC and for the modelling of the NEPTUNE_CFD code developed by CEA, EDF and sponsored by AREVA-NP and IRSN.

Appendix A. Modelling of the coalescence and break-up effects in the different approaches

A.1. Single-size approach: model of Wu et al. (1998)

In this section, we summarize the model of Wu et al. (1998) for the source terms due to coalescence and break-up $B_0^{+/-}$ and $C_0^{+/-}$ appearing in the RHS of Eq. (18). The bubble break-up is assumed to be due to the impact of bubbles with the liquid turbulent eddies. The bubble break-up source and sink terms are modelled together in a single source term:

$$B_0 \hat{=} B_0^+ - B_0^- = C_{TI} \exp\left(-\frac{We_{cr}}{We}\right)\sqrt{1-\frac{We_{cr}}{We}}\frac{n}{d_{32}}(\varepsilon_L d_{32})^{1/3} \quad \text{with :}$$
$$We \hat{=} \frac{\rho_L \varepsilon_L^{2/3} d_{32}^{5/3}}{\sigma}, \qquad We_{cr} = 2, \qquad C_{TI} = 0.18 \tag{A.1}$$

where We and We_{cr} are the Weber number and its critical value (bubble break-up occurs only if $We > We_{cr}$). The coefficient C_{TI} is a fitted constant, ρ_L and σ are the liquid density and the surface tension, respectively, and ε_L is the mean turbulent dissipation rate in the liquid, which is given by the solution of a liquid K–ε model in our work.

The coalescence terms are supposed to result from two different collision sources. The first one are the random collisions due to the entrainment of bubbles by liquid turbulent eddies, these eddies having approximately the same size than the bubbles. The second source of bubble collisions is by wake entrainment, when a bubble is entrapped into the wake of a preceding bubble. Denoting by RC the bubble coalescence due to random collisions and by WE the bubble coalescence due to wake entrainment, we can write:

$$C_0 \hat{=} C_0^+ - C_0^- = -C_{0,RC} - C_{0,WE} \tag{A.2}$$

The authors modelled these two sinks of bubbles caused by coalescence by the following relations:

$$C_{0,RC} = \frac{C_{RC}(\varepsilon_L d_{32})^{1/3} n^2 d_{32}^2}{\alpha_{max}^{1/3}(\alpha_{max}^{1/3} - \alpha^{1/3})}\left[1 - \exp\left(-C\frac{\alpha_{max}^{1/3}\alpha^{1/3}}{\alpha_{max}^{1/3} - \alpha^{1/3}}\right)\right] \quad \text{with :}$$
$$C_{RC} = 0.0565, \qquad C = 3, \qquad \alpha_{max} = 0.65 \tag{A.3}$$

where C_{RC} and C are two fitted constants, α is the void fraction and α_{max} is the dense packing limit of the void fraction. For spherical bubbles stacked in a hexagonal close-packed structure, α_{max} is equal to 0.65 and the model (A.3) is valid only for $\alpha < \alpha_{max}$ (the coalescence rate approaches infinity when α approaches α_{max}). The coalescence rate due to wake entrainment is given by the following relation:

$$C_{0,WE} = C_{WE} d_{32}^2 n^2 u_r(d_{32}) \qquad \text{with :}$$
$$C_{WE} = 0.151, \qquad u_r(d_{32}) = \sqrt{\frac{4}{3}\frac{|\rho_L - \rho_G| g d_{32}}{\rho_L C_D}} \tag{A.4}$$

where C_{WE} is a fitted constant and $u_r(d_{32})$ is the terminal velocity of a bubble having a diameter d_{32}, obtained by matching the weight and Archimedes forces exerted on the bubble to the bubble drag force, C_D being the drag coefficient.

A.2. Coalescence modelling in the context of the log–normal law

Here we summarize the coalescence model derived by Kamp et al. (2001) when the bubble diameter distribution function is modelled by a log–normal law. The break-up integrals diverge using such a distribution function (Riou, 2003). The coalescence terms appearing in Eqs. (24) for the two particular moments S_1 and S_2 read:

$$C_1 \hat{=} C_1^+ - C_1^- = K_C\sqrt{\frac{8\pi}{3}}\left(\frac{6\alpha}{\pi}\right)^{2/3}\frac{C_t \varepsilon_L^{1/3}}{\sqrt{1.61}}(2^{1/3} - 2)S_1^{4/3}F(1, \hat{\sigma}, P_{00})$$
$$C_2 \hat{=} C_2^+ - C_2^- = K_C\sqrt{\frac{8\pi}{3}}\left(\frac{6\alpha}{\pi}\right)^{1/3}\frac{C_t \varepsilon_L^{1/3}}{\sqrt{1.61}}(2^{2/3} - 2)S_2^{5/3}F(2, \hat{\sigma}, P_{00}) \tag{A.5}$$

In these equations, K_C is a fitted constant equal to 1, the coefficient C_t is the ratio between the dispersed phase velocity fluctuations and the continuous phase velocity fluctuations, ε_L is the mean liquid turbulent dissipation rate which is given here by the solution of a K–ε model used for the liquid phase, $F(1, \hat{\sigma}, P_{00})$ and $F(2, \hat{\sigma}, P_{00})$ are power law functions of the width parameter $\hat{\sigma}$ and P_{00}. The quantity P_{00} is the coalescence probability of two bubbles having the diameter d_{00}. All the details are given in the paper from Kamp et al. (2001).

A.3. Coalescence and break-up modelling in the context of the quadratic law

In the context of the moments method using the quadratic law (25) for the bubble diameter distribution function, the IAC balance equation $(15)_3$ must be solved in order to close the system. The coalescence and break-up terms appearing in this equation can be rewritten (Ruyer, 2008):

$$\pi(B_2^+ - B_2^- + C_2^+ - C_2^-) = \int\int \frac{\pi}{2}[(d_1^3 + d_2^3)^{2/3} - d_1^2 - d_2^2] f_{coal}(d_1, d_2)\, \delta d_1 \delta d_2 + \int \pi(2^{1/3} - 1) d^2 f_{break\text{-}up}(d)\delta d \tag{A.6}$$

where $f_{coal}(d_1,d_2)$ and $f_{break\text{-}up}(d)$ are coalescence and break-up frequencies. The modelled expression for the IAC source terms by coalescence reads:

$$\pi(C_2^+ - C_2^-) = a_i^{5/3}\varepsilon_L^{1/3}\alpha^{1/3}\xi(N_c)$$
$$\text{with} \quad \xi(N_c) = -0.18(1 + 0.341N_c + 0.199N_c^2)\exp(-0.561N_c)$$
$$\text{and} \quad N_c \hat{=} 8.06\left(\frac{\alpha}{a_i}\right)^{5/6}\varepsilon_L^{1/3}\sqrt{\frac{\rho_L}{\sigma}} \tag{A.7}$$

The break-up term is derived from the original model from Wu et al. (1998) rewritten in the context of the quadratic law for the bubble size distribution. The source term in the IAC balance equation reads:

$$\pi(B_2^+ - B_2^-) = 3.01\,\frac{\alpha\rho_L\varepsilon_L}{\sigma \mathrm{We}_{\mathrm{cr}}}\,\frac{\widetilde{X}-1}{\widetilde{X}^2}\exp\left(-\frac{2}{\widetilde{X}}\right)\sqrt{1-\frac{1}{\widetilde{X}}}$$
$$\text{with} \quad \widetilde{X} \hat{=} \left(\frac{2d_{10}}{d_{\mathrm{cr}}}\right)^{5/3} \quad \text{where} \quad d_{\mathrm{cr}} \hat{=} \left(\frac{\sigma \mathrm{We}_{\mathrm{cr}}}{\rho_L\varepsilon_L^{2/3}}\right)^{3/5} \quad \text{and} \quad \mathrm{We}_{\mathrm{cr}} = 2 \tag{A.8}$$

In these relations, d_{cr} denotes the critical bubble diameter corresponding to the critical Weber number. Bubbles having their diameter smaller than d_{cr} do not break-up, hence the model (A.8) must be used only for $\widetilde{X}$ values larger than 1.

A.4. Coalescence and break-up modelling in the context of the multi-field model

Here we must propose some closure relations for the inter-class mass transfer terms B_i^+, B_i^-, C_i^+ and C_i^- appearing in the mass balance equation (42). We have adapted the discrete expressions proposed by Carrica et al. (1999) into the following form:

$$\begin{aligned} B_i^+ &= \sum_{j=i+1}^{N} b_j\alpha_{g,j}\rho_{g,j}X_{i,j} \\ B_i^- &= b_i\alpha_{g,i}\rho_{g,i} \\ C_i^+ &= \frac{\rho_{g,i}}{2}\sum_{j=1}^{i-1} c_{j,i-j}\alpha_{g,j}\alpha_{g,i-j}X_{i,j,i-j} \\ C_i^- &= \rho_{g,i}\sum_{j=1}^{N-i} c_{i,j}\alpha_{g,i}\alpha_{g,j} \end{aligned} \tag{A.9}$$

where $\alpha_{g,i}$ and $\rho_{g,i}$ are the void fraction and the density characterizing the bubble class i, b_i and $c_{i,j}$ are *break-up and coalescence frequencies* and $X_{i,j}$ and $X_{i,j,k}$ are non-dimensional matrices guaranteeing that the coalescence and break-up do not change the total amount of gas according to Carrica et al. (1999). These authors proposed some expressions for the matrices $X_{i,j}$ and $X_{i,j,k}$ but in fact, we do not need to retain exactly their expressions, as it will be shown. The total void fraction conservation by the coalescence and break-up phenomena reads:

$$\sum_{i=1}^{N}\left(\sum_{j=i+1}^{N} b_j\alpha_{g,j}\rho_g X_{i,j} - b_i\alpha_{g,i}\rho_g + \frac{\rho_g}{2}\sum_{j=1}^{i-1} c_{j,i-j}\alpha_{g,j}\alpha_{g,i-j}X_{i,j,i-j} - \rho_g\sum_{j=1}^{N-i} c_{i,j}\alpha_{g,i}\alpha_{g,j}\right) = 0 \tag{A.10}$$

It has been assumed that the gas density is the same for all the bubble classes. Eq. (A.10) is simply obtained by summing $B_i^+ - B_i^- + C_i^+ - C_i^-$ on the N classes. Eq. (A.10) thus guarantees that the coalescence and break-up terms disappear when summing the mass balance equations (34) for the N classes, in order to obtain the total gas mass balance equation (37). As coalescence and break-up are two separate (independent) phenomena, each of them must verify (A.10) independently of the other. Let us first examine the consequence of (A.10) for the coalescence terms. Developing the sums in the last two terms of (A.10) and assuming that the their sum on the N classes should cancel for each value of $c_{i,j}$ independently, we obtain the following conditions for the first few classes:

$$\begin{aligned} &X_{2,1,1} = X_{4,2,2} = 2 \\ &X_{3,1,2} + X_{3,2,1} = 4 \\ &X_{4,1,3} + X_{4,3,1} = 4 \\ &\dots \end{aligned} \tag{A.11}$$

A mathematical induction shows that it is sufficient to make the following choice:

$$X_{i,j,i-j} = 2 \quad \forall i,j \tag{A.12}$$

to guarantee the total gas mass conservation by the coalescence phenomenon.

Reasoning in the same manner on the break-up phenomenon, i.e. supposing that the break-up terms in (A.10) should sum to zero for each frequency b_i independently, we obtain for the first few classes:

$$\begin{aligned} &b_1 = 0 \\ &b_2\alpha_2(X_{12} - 1) = 0 \\ &b_3\alpha_3(X_{13} + X_{23} - 1) = 0 \\ &b_4\alpha_4(X_{14} + X_{24} + X_{34} - 1) = 0 \\ &\dots \end{aligned} \tag{A.13}$$

Mathematical induction shows that this is equivalent to impose:

$$\sum_{j=1}^{i-1} X_{j,i} = 1 \quad i = 2, N \quad \text{and} \quad b_1 = 0 \tag{A.14}$$

For the NEPTUNE_CFD code implementation, however, we do not need to verify Eq. (A.14) (except for $b_1 = 0$ which expresses that the bubbles in the smallest diameter class are not allowed to break-up), because the algorithm for the inter-class mass transfers automatically guarantees the total mass conservation. This is simply done by considering the gas fields by pairs and, for each mass exchange between two bubble classes, to impose that the mass source in one of the two bubble classes is exactly equal to the mass sink in the other one. Therefore we keep a freedom degree on the expression of the matrix $X_{i,j}$. Several expressions have been tested and we have retained the one giving the smoothest bubble diameter distribution function. This expression reads:

$$X_{i,j} = v_i/v_j \tag{A.15}$$

where v_j and v_i are the volumes of the parent bubble and the daughter bubble, respectively. Despite the fact that (A.15) gives a value of $X_{i,j}$ that is smaller than 1, it does not respect Eq. (A.14) but, as it has been explained, this does not influence the total gas mass conservation in the NEPTUNE_CFD code due to the particular algorithm used for the mass exchanges between different phases or fields. Retaining the value given by (A.12) for the coalescence matrix into the model (A.9) and comparing this model to the general algorithm for mass exchanges between two phases in NEPTUNE_CFD, the implemented mass exchange term for coalescence and break-up reads:

$$\mathrm{TS}_{i,j} = b_j\alpha_j\rho_g X_{i,j} - \rho_g c_{i,j-i+1}\alpha_i\alpha_{j-i+1} \qquad i = 2, N \quad \text{and} \quad j = i+1, N+1 \tag{A.16}$$

where $\mathrm{TS}_{i,j}$ is the mass exchange term between phases i and j, directed from j towards i when it is positive. The shift of the indices is due to the fact that the phase 1 is occupied by the liquid, therefore the N gas fields are numbered from 2 to $N+1$.

Now, we must give some closed expressions for the coalescence and break-up frequencies. According to Prince and Blanch (1990), the coalescence rate between a first bubble population having a diameter d_i and characterized by a bubble number density n_i, with a second bubble population having a diameter d_j and characterized by a bubble number density n_j is given by the following equation:

$$\left.\frac{\partial n_i}{\partial t}\right|_{\text{coal}} = -n_i n_j S_{ij} V_{ij}^c \eta_{ij}^c \tag{A.17}$$

where S_{ij} is the collision cross-sectional area of bubbles, V_{ij}^c is the collision velocity and η_{ij}^c is the coalescence efficiency. Introducing $\alpha_{g,i} = n_i v_i$ and $\alpha_{g,j} = n_j v_j$ where v_i and v_j denote the volumes of the two bubble classes considered, Eq. (A.17) can be rewritten as:

$$\left.\frac{\partial \alpha_{g,i}\rho_g}{\partial t}\right|_{\text{coal}} = -\rho_g \frac{\alpha_{g,i}\alpha_{g,j}}{v_j} S_{ij} V_{ij}^c \eta_{ij}^c \tag{A.18}$$

Shifting the phase index as previously mentioned ($\alpha_{g,i-1} = \alpha_i$), and comparing (A.18) to (A.16), the mass transfer term between the fields i and j due to coalescence reads:

$$\text{TS}_{i,j} = -\rho_g c_{i,j-i+1}\alpha_i\alpha_{j-i+1} = -\rho_g \frac{\alpha_i\alpha_{j-i+1}}{v_{j-i+1}} S_{i,j-i+1} V_{i,j-i+1}^c \eta_{i,j-i+1}^c \tag{A.19}$$

from which the coalescence frequency between the two bubble classes i and $(j - i + 1)$ is deduced:

$$c_{i,j-i+1} = \frac{S_{i,j-i+1}}{v_{j-i+1}} V_{i,j-i+1}^c \eta_{i,j-i+1}^c \tag{A.20}$$

Hence, the coalescence terms in Eq. (42) are completely close if one adopts some expressions for the three quantities $S_{i,j-i+1}$, $V_{i,j-i+1}^c$ and $\eta_{i,j-i+1}^c$. Several expressions are available in the literature for these quantities. Here, these quantities were modelled according to Wu et al. (1998) for the two possible sources of coalescence: by random collisions (RC) and by wake entrainment (WE).

The same kind of reasoning leads to the following expression for the break-up frequency of a bubble belonging to the class j:

$$b_j = \frac{\eta_j^b}{t_j^b} \tag{A.21}$$

where η_j^b and t_j^b denote a break-up efficiency and a characteristic time for bubble break-up, respectively. Several expressions are available in the literature for these quantities. Here we have retained the expressions similar to those of Wu et al. (1998) for bubble break-up due to turbulent impact (TI).

Appendix B. Brief description of the K–ε model for bubbly flows

The Reynolds stress tensor for the liquid phase is assumed to be given by the usual closure relation (e.g. Schiestel, 1993):

$$\tau_{L_{ij}}^T = \rho_L \nu_L^T (V_{L_{i,j}} + V_{L_{j,i}}) - \frac{2}{3}\delta_{ij}(\rho_L K_L + \rho_L \nu_L^T V_{L_{l,l}}) \tag{B.1}$$

In this relation, ν_L^T is the turbulent eddy viscosity, which is also assumed to be given by the "single-phase" closure relation:

$$\nu_L^T = C_\mu \frac{K_L^2}{\varepsilon_L} \tag{B.2}$$

where C_μ is a model constant equal to 0.09. The liquid turbulent kinetic energy K_L and its dissipation rate ε_L are calculated by their "two-phase" transport equations:

$$\begin{aligned}&\frac{\partial(1-\alpha)\rho_L K_L}{\partial t} + \nabla.[(1-\alpha)\rho_L K_L \underline{V}_L] \\ &= \nabla.\left[(1-\alpha)\rho_L \frac{\nu_L^T}{\sigma_K}\nabla K_L\right] - (1-\alpha)\underline{\underline{\tau}}_L^T : \underline{\underline{\nabla}}\underline{V}_L - (1-\alpha)\rho_L\varepsilon_L + P_K^i\end{aligned} \tag{B.3}$$

$$\begin{aligned}&\frac{\partial(1-\alpha)\rho_L \varepsilon_L}{\partial t} + \nabla.[(1-\alpha)\rho_L \varepsilon_L \underline{V}_L] \\ &= \nabla.\left[(1-\alpha)\rho_L \frac{\nu_L^T}{\sigma_\varepsilon}\nabla\varepsilon_L\right] - C_{\varepsilon 1}\frac{\varepsilon_L}{K_L}(1-\alpha)\underline{\underline{\tau}}_L^T : \underline{\underline{\nabla}}\underline{V}_L \\ &\quad - C_{\varepsilon 2}(1-\alpha)\rho_L\frac{\varepsilon_L^2}{K_L} - \frac{2}{3}(1-\alpha)\rho_L\varepsilon_L\nabla.\underline{V}_L + P_\varepsilon^i\end{aligned} \tag{B.4}$$

The exact counterpart of the modelled equations (B.3) and (B.4) have been derived in a previous paper (Morel, 1995). An order of magnitude analysis of these exact equations followed by a comparison to several experimental bubbly flows allowed us to greatly simplify these balance equations. At the end, we arrived to the simplified equations (B.3) and (B.4) where the terms P_K^i and P_ε^i represent the remaining interfacial interaction terms in the K and ε equations, respectively. Therefore, even if the closure relations for the Reynolds stress tensor (B.1) and for the eddy viscosity (B.2) are "single-phase" relations, the two-phase aspects due to the presence of the bubbles are taken into account in two different manners. First, the liquid does not occupy the total space of the flow domain because it must share this space with the second gaseous phase. This is taken into account by the presence of the liquid fraction of presence $(1 - \alpha)$ in the different terms of Eqs. (B.3) and (B.4). Second, the two terms P_K^i and P_ε^i take into account the liquid turbulence modulation by the bubbles. For this second aspect, a very simple model has been adopted. The term P_K^i is supposed to be a source of liquid turbulent kinetic energy due to the turbulent wakes behind the bubbles in their relative movement. It is modelled by the power developed by the averaged drag force in the relative velocity:

$$P_K^i = -\underline{M}_G^D.(\underline{V}_G - \underline{V}_L) \tag{B.5}$$

After being produced, this additional turbulent kinetic energy is dissipated through the term P_ε^i in the liquid dissipation rate balance equation. This additional dissipation is assumed to be characterized by a time τ constructed with the averaged liquid dissipation rate and the Sauter mean bubble diameter:

$$P_\varepsilon^i = C_{\varepsilon_3}\frac{P_K^i}{\tau} \qquad \tau = \left(\frac{d_{32}^2}{\varepsilon_L}\right)^{1/3} \tag{B.6}$$

Appendix C. Supplementary data

Supplementary data associated with this article can be found, in the online version, at doi:10.1016/j.ijmultiphaseflow.2009.09.003.

References

Achard, J.L., 1978. Contribution à l'étude théorique des écoulements diphasiques en régime transitoire. Thèse de Doctorat, Université Scientifique et Médicale, Institut National Polytechnique Grenoble.

Antal, S.P., Lahey Jr., R.T., Flaherty, J.E., 1991. Analysis of phase distribution in fully developed laminar bubbly two-phase flow. Int. J. Multiphase Flow 17, 635–652.

Auton, T.R., 1987. The lift force on a spherical body in a rotational flow. J. Fluid Mech. 183, 199–218.

Carrica, P.M., Drew, D., Bonetto, F., Lahey Jr., R.T., 1999. A polydisperse model for bubbly two-phase flow around a surface ship. Int. J. Multiphase Flow 25, 257–305.

Chen, P., Dudukovic, M.P., Sanyal, J., 2005. Three-dimensional simulation of bubble column flows with bubble coalescence and break-up. AIChE J. 51, 696–712.

Colin, C., Riou, X., Fabre, J., 2004. Turbulence and shear-induced coalescence in gas-liquid pipe flows. In: Fifth International Conference on Multiphase Flow, ICMF'04, Yokohama, Japan, May 30–June 4, Paper No. 425.

Doi, M., Ohta, T., 1991. Dynamics and rheology of complex interfaces. J. Chem. Phys. 95, 1242–1248.

Drew, D.A., Passman, S.L., 1999. Theory of Multicomponent Fluids. In: Applied Mathematical Sciences, vol. 135. Springer.

Guido-Lavalle, G., Clausse, A., 1991. Application of the statistical description of two-phase flows to interfacial area assessment. In: VIII ENFIR, Atibaia, SP, Septembro, pp. 143–146.

Guido-Lavalle, G., Carrica, P., Clausse, A., Qazi, M.K., 1994. A bubble number density constitutive equation. Nucl. Eng. Des. 152, 213–224.

Hibiki, T., Ishii, M., 2000. One-group interfacial area transport of bubbly flows in vertical round tubes. Int. J. Heat Mass Transfer 43, 2711–2726.

Hulburt, H.M., Katz, S., 1964. Some problems in particle technology: a statistical mechanical formulation. Chem. Eng. Sci. 19, 555–574.

Ishii, M., 1990. Two-fluid model for two-phase flow. Multiph. Sci. Technol. 5, 1–58.

Ishii, M., Kim, S., 2001. Micro four-sensor probe measurement of interfacial area transport for bubbly flow in round pipes. Nucl. Eng. Des. 205, 2711–2726.

Ishii, M., Hibiki, T., 2006. Thermo-Fluid Dynamics of Two-Phase Flow. Springer.

Kalkach-Navarro, S., Lahey Jr., R.T., Drew, D.A., 1994. Analysis of the bubbly/slug flow regime transition. Nucl. Eng. Des. 151, 15–39.

Jones, I.P., Guilbert, P.W., Owens, M.P., Hamill, I.S., Montavon, C.A., Penrose, J.M.T., Prast, B., 2003. The use of coupled solvers for complex multi-phase and reacting flows. In: Third International Conference on CFD in the Minerals and Process Industries, CSIRO, Melbourne, Australia, 10–12 December.

Kamp, A.M., 1996. Ecoulements turbulents à bulles dans une conduite en micropesanteur. Thèse de Doctorat, Institut National Polytechnique de Toulouse.

Kamp, A.M., Chesters, A.K., Colin, C., Fabre, J., 2001. Bubble coalescence in turbulent flows: a mechanistic model for turbulence induced coalescence applied to microgravity bubbly pipe flow. Int. J. Multiphase Flow 27, 1363–1396.

Kocamustafaogullari, G., Ishii, M., 1995. Foundation of the interfacial area transport equation and its closure relations. Int. J. Heat Mass Transfer 38, 481–493.

Krepper, E., Lucas, D., Shi, J.M., Prasser, H.M., 2006. Simulations of FZR adiabatic air–water data with CFX-10. Nuresim European Project, D.2.2.3.1.

Lamb, H., 1932. Hydrodynamics, sixth ed. Dover Publications, New York.

Lhuillier, D., Morel, C., Delhaye, J.M., 2000. Bilan d'aire interfaciale dans un mélange diphasique: approche locale vs approche particulaire. C. R. Acad. Sci. II B (Paris) 328, 143–149.

Lhuillier, D., 2004a. Small-scale and coarse-grained dynamics of interfaces: the modeling of volumetric interfacial area in two-phase flows. In: Third International Symposium on Two-Phase Flow Modelling and Experimentation, Pisa, Italy, 22–24 September.

Lhuillier, D., 2004b. Evolution de la densité d'aire interfaciale dans les mélanges liquide-vapeur. C. R. Mech. 332, 103–108.

Lucas, D., Krepper, E., Prasser, H.M., 2001. Modeling of radial gas fraction profiles for bubble flow in vertical pipes. In: Ninth International Conference on Nuclear Engineering (ICONE-9), Nice, France, April 2001.

Lucas, D., Krepper, E., Prasser, H.M., 2005. Development of co-current air–water flow in a vertical pipe. Int. J. Multiphase Flow 31, 1304–1328.

Lucas, D., Krepper, E., 2007. CFD models for polydispersed bubbly flows. Technical Report FZD-486.

Morel, C., 1995. An order of magnitude analysis of the two-phase K–ε model. Int. J. Fluid Mech. Res. 22, 21–44.

Morel, C., Pouvreau, J., Laviéville, J., Boucker, M., 2004. Numerical simulations of a bubbly flow in a sudden expansion with the NEPTUNE code. In: Third International Symposium on Two-Phase Flow Modeling and Experimentation, Pisa, Italy, September 22–24.

Morel, C., Mimouni, S., Laviéville, J., Boucker, M., 2005. R113 boiling bubbly flow in an annular geometry simulated with the NEPTUNE code. In: The Eleventh International Topical Meeting on Nuclear Reactor Thermal-Hydraulics (NURETH-11), Paper No. 248, Popes' Palace Conference Center, Avignon, France, October 2–6, 2005.

Morel, C., 2007. On the surface equations in two-phase flows and reacting single-phase flows. Int. J. Multiphase Flow 33, 1045–1073.

Morel, C., Laviéville, J., 2008. Modeling of multi-size bubbly flow and application to the simulation of boiling flows with the NEPTUNE_CFD code. In: Science and Technology for Nuclear Installations, vol. 2009. Article ID 953527. doi:10.1155/2009/953527.

Mossa, J.B., 2005. Extension polydisperse pour la description Euler–Euler des écoulements diphasiques réactifs. Thèse de Doctorat, Institut National Polytechnique de Toulouse.

Oesterlé, B., 2006. Ecoulements multiphasiques. Hermès, Lavoisier.

Prince, M.J., Blanch, H.W., 1990. Bubble coalescence and break-up in air-sparged bubble columns. AIChE J. 36, 1485–1499. 99.

Riou, X., 2003. Contribution à la modélisation de l'aire interfaciale en écoulement gaz-liquide en conduite. Thèse de Doctorat, Institut National Polytechnique de Toulouse.

Ruyer, P., Seiler, N., Beyer, M., Weiss, F.P., 2007. A bubble size distribution model for the numerical simulation of bubbly flows. In: Sixth International Conference Multiphase Flow, ICMF2007, Leipzig, Germany, July 9–13.

Ruyer, P., 2008, Modélisation de la polydispersion en taille: méthode des moments appliquée aux écoulements adiabatiques à bulles. IRSN, NT SEMCA 2008-047.

Seiler, N., Ruyer, P., 2008. Advanced model for polydispersion in size in boiling flows. In: 190ieme session du comité scientifique et technique de la société hydrotechnique de France, Modélisation des écoulements diphasiques bouillants, Grenoble, 8–9 septembre.

Schiestel, R., 1993. Modélisation et simulation des écoulements turbulents. Hermès.

Sha, Z., Laari, A., Turunen, I., 2006. Multi-Phase-Multi-Size-Group model for the inclusion of population balances into the CFD simulation of gas–liquid bubbly flows. Chem. Eng. Technol. 29.

Tomiyama, A., 1998. Struggle with computational bubble dynamics. In: Third International Conference Multiphase Flow ICMF'98, Lyon, France, June 8–12.

Tomiyama, A., Shimada, N., 1998. Numerical simulations of bubble columns using a 3D multi-fluid model. In: Third International Conference Multiphase Flow ICMF'98, Lyon, France, June 8–12.

Wellek, R.M., Agrawal, A.K., Skelland, A.H.P., 1966. Shapes of liquid drops moving in liquid media. AIChE J. 12, 854–860.

Wetzel, E.D., Tucker, C.L., 1999. Area tensors for modeling microstructure during laminar liquid–liquid mixing. Int. J. Multiphase Flow 25, 35–61.

Wu, Q., Kim, S., Ishii, M., Beus, S.G., 1998. One-group interfacial area transport in vertical bubble flow. Int. J. Heat Mass Transfer 41, 1103–1112.

Yao, W., Morel, C., 2004. Volumetric interfacial area prediction in upward bubbly two-phase flow. Int. J. Heat Mass Transfer 47, 307–328.

Zuber, N., 1964. On the dispersed two-phase flow in the laminar flow regime. Chem. Eng. Sci. 19, 897.